INSTITUTO SUPERIOR TÉCNICO
Universidade Técnica de Lisboa

Characterisation of the Radio Channel in On-Body Communications

Carlos Alexandre da Graça Lopes

Dissertation submitted for obtaining the degree of
Master in Electrical and Computer Engineering

Jury

Supervisor:	Prof. Luis Manuel de Jesus Sousa Correia
President:	Prof. José Manuel Bioucas Dias
Members:	Prof. Custódio José de Oliveira Peixeiro

November 2010

To *my beloved ones*

Acknowledgements

First of all I would like to thank my mother because everything that I have, I owe it to her. She was capable of raising me, my brother and my sister, all by herself and without her I certainly would not be where I am right now.

I would like to thank Prof. Luís Correia for giving me the opportunity to work with him. All his experience and knowledge are undoubtedly one advantage for everyone who works with him, and I felt that in all the phases of my McS Thesis. For all his help I want to express my sincere gratitude.

I must also thank Carla Oliveira and Michal Maćkowiak, despite all the work and time consumption underlying a PhD, they were essential to the development of my thesis with all their help and advices.

To my longtime friends, André Calvinho, João Rodrigues and Raquel Costa who gave me advices and opinions during the thesis writing.

To my beloved girlfriend Marta, for all the emotional support and patience during this period.

To all my family and friends.

Abstract

This MsC Thesis takes in hand the study of Body Area Networks (BANs) and Private Area Networks (PANs), more accurately the Characterisation of the Radio Channel in On-Body Communications.

In this MsC Thesis it is analised the influence of the human body, both in the characteristics of a specific antenna, as well as, in the characterization of the rádio channel between two antennas disposed on the body.

The simulator *CST Studio Suite 2010* uses Finite Integration Technique (FIT), being the reason why it was the simulation tool used to perform a statistical study of how the antenna characteristics vary with the distance to the body, as well as, simulations to characterise the radio channel.

The measurements of the radio channel were performed in the anechoic chamber with three individuals in several body postures and with the antennas placed in several body parts, while the radiation pattern measurements were carried out with the antenna placed on the chest.

Results are concordant with each other, being that the influence of the body in the antenna characteristics is small, while its influence in the radio channel between two antennas disposed on the body is quite substantial, when compared with free space propagation.

Keywords

Body Area Network, Private Area Network, CST, Finite Integration Technique, Anechoic Chamber.

Resumo

Esta Tese de Mestrado estuda Redes na Área do Corpo Humano e Redes de Área Pessoal, mais precisamente a Caracterização do Canal Rádio em Comunicações na Superfície do Corpo Humano.

Esta Tese de Mestrado trata a problemática da influência do corpo humano, tanto nas características de uma antena específica, assim como na caracterização do canal rádio entre duas antenas dispostas ao longo do corpo.

O simulador *CST Studio Suite 2010* usa a Técnica de Integração Finita, sendo essa a razão pela qual foi o simulador escolhido para realizar o estudo estatístico da variação das características da antena com a distância a que se encontram do corpo humano, assim como, simulações para caracterizar o canal rádio.

As medições foram realizadas na câmara anecóica em três indivíduos, em várias posturas e com as antenas em diferentes partes do corpo, enquanto as medições dos diagramas de radiação foram feitas com a antena colocada no peito.

Observando os resultados, pode-se ver que são concordantes, sendo a influência do corpo nas características da antena pequena, ao passo que a sua influência no canal rádio entre as duas antenas colocados no corpo é bastante significativo, quando comparando com a atenuação em espaço livre.

Palavras-chave

Câmara Anecóica, Redes na Área do Corpo Humano, Redes de Área Pessoal, CST, Técnica de Integração Finita.

Table of Contents

Acknowledgements v

Abstract vii

Resumo viii

Table of Contents ix

List of Figures xi

List of Tables xiii

List of Acronyms xiv

List of Symbols xvi

List of xviii

1 Introduction 1

1.1 Overview 2

2 Body-centric communications 7

2.1 Body-centric communications and frequency bands 8

2.1.1 Body-centric communications categories 8

2.1.2 Systems frequency bands and applications 9

2.2 Human body characterisation and modelling 11

2.2.1 Dielectric properties 11

2.2.2 Phantoms 12

2.3 Numerical modelling techniques 14

2.3.1 Modelling techniques 14

2.3.2 Error Sources 18

2.4 Antennas and propagation 19

2.4.1 Propagation Mechanisms 19

2.4.2 Antennas 21

3 Modelling and Simulation 25

3.1 Problem Description and Model 26

3.2 CST Simulator 27
3.3 Resolution Assessment 31
3.3.1 Assessment Parameters 31
3.3.2 Scenario 33
3.3.3 Assessment Results 34
4 Analysis of Results 39
4.1 Scenarios Definition 40
4.2 Simulations Results 45
4.2.1 Radiation Patterns and Antenna Characteristics 45
4.2.2 Path Loss 50
4.3 Measurements Results 51
4.3.1 Radiation Patterns 51
4.3.2 Path Loss 54
4.4 Comparison 60
5 Conclusions 61
Annex 1 - Dielectric Properties of Body Tissues 65
Annex 2 - Voxel Models Body Parts 68
Annex 3 - Different Body Postures in Path Loss Measurements 74
References 81

List of Figures

Fig 1.1. Representation of a BAN and all the backbone with which the BAN may be connected. (extracted from [Wica10]) 3
Fig 2.1. Representation of the influence area of a BAN, a PAN and points of care (extracted from [HaoY09]) 8
Fig 2.2. High-resolution female whole-body human voxel model (extracted from [CSTM10]). 14
Fig 2.3. Representation of the leapfrog arrangement (extracted from [CSTH10]). 17
Fig 2.4. Measured belt-to-chest path gain with monopole to disc monopole antennas (solid line) and monopole to monopole antennas (dotted line) at 2.45 GHz (extracted from [HaHa06a]) 21
Fig 3.1. Division of the human body 27
Fig 3.2. Representation the grid division and allocation of grid voltages and facet fluxes. 29
Fig 3.3. Graphic representation of the discretisation of Maxwell's integral equations (extracted from [CSTH10]). 29
Fig 3.4. Patch antenna with switchable slots in a closed configuration (extracted from [MeCa06]). 34
Fig 3.5. Radiation pattern of patch antenna in free space and near to the head model. 36
Fig 3.6. Radiation patterns of the different meshing. 37
Fig 3.7. Representation of the relative errors' module for each meshing. 38
Fig 4.1. Antenna radiation pattern measurements. 41
Fig 4.2. Measuring setup of the radiation patterns. 42
Fig 4.3. Radio link between the arm and the chest. 42
Fig 4.4. Radio link between the arm and the head. 43
Fig 4.5. Radio link between the arm and the leg. 43
Fig 4.6. Female voxel model chest, with antenna placed in the middle of the chest. 46
Fig 4.7. Female voxel model left leg, with the antenna placed on the left side. 46
Fig 4.8. Female voxel model head, with the antenna placed on the left ear 46
Fig 4.9. Female voxel model left arm, with the antenna placed on the wrist. 47
Fig 4.10. Average value of the reflection coefficient, S_{11}, for each body part, when varying the distance of the antenna from the body [0, 2 λ]. 47
Fig 4.11. Average value of the antenna efficiency for each body part, when varying the distance of the antenna from the body [0, 2 λ]. 48
Fig 4.12. Average value of the antenna gain for each body part, when varying the distance of the antenna from the body [0, 2 λ]. 49
Fig 4.13. Maximum, minimum, average radiation patterns near the body parts and the radiation pattern of the antenna in free space. 50
Fig 4.14. Antennas' radiation pattern on CO's body 52
Fig 4.15. Antennas' radiation pattern on CA's and MM' body. 52
Fig 4.16. Antennas' radiation pattern at the same distance of the body. 53
Fig 4.17. Reflection Coefficients mean values for each body posture. 55
Fig 4.18. Path Loss of all the measurements performed, considering all positions and all three individuals. 58
Fig 4.19. Path Loss of all the measurements performed, considering all positions and all three individuals, differentiating between QLOS and NLOS radio channels. 59

Fig A1.1. Conductivity of the most important body tissues. 66
Fig A1.2. Relative permittivity of the most important body tissues. 66
Fig A1.3. Penetration depths of the most important body tissues. 67

Fig A2.1. Antennas' Radiation Pattern with antenna in free space. 69
Fig A2.2. Antennas' Radiation Pattern with antenna 12 mm away from the arm. 69
Fig A2.3. Antennas' Radiation Pattern with antenna 2 λ (245 mm) away from the arm.. 70
Fig A2.4. Antennas' Radiation Pattern with antenna 12 mm away from the chest. 70
Fig A2.5. Antennas' Radiation Pattern with antenna 2 λ (245 mm) away from the chest.. 71
Fig A2.6. Antennas' Radiation Pattern with antenna 12 mm away from the head.. 71
Fig A2.7. Antennas' Radiation Pattern with antenna 2 λ (245 mm) away from the head.. 72
Fig A2.8. Antennas' Radiation Pattern with antenna 12 mm away from the leg. 72
Fig A2.9. Antennas' Radiation Pattern with antenna 2 λ (245 mm) away from the leg.. 73

Fig A3.1. Standing up with the arm down, perpendicular to the soil (STD_ADOWN). 75
Fig A3.2. Standing up with the arm parallel to the soil (STD_AFRONT)... 75
Fig A3.3. Standing up with the arm up, approximately 45º higher than with the arm parallel to the soil (STD_AUP). 76
Fig A3.4. Standing up with the arm on the back side of the body, similar to when a person is walking and swings the arms (STD_ABACK). 76
Fig A3.5. Sitting down with the arm down (SIT_ADOWN) 77
Fig A3.6. Sitting down bending the elbow 90º (SIT_ABEND). 77
Fig A3.7. Intermediate position between standing up and knelling with just one knee on the ground as explained in the previous mark (MIL_STEP) 78
Fig A3.8. Kneeling with just one knee on the ground and with the arms in front of the body simulating that is holding a rifle (MIL_KNEE) 78

List of Tables

Table 2.1. List of all possible scenarios and their descriptions (extracted from [YaSa09]) 11
Table 3.1. Tissues properties in the extremes of the studied frequency band. 33
Table 3.2. Statistic data from the optimisation assessment 35
Table 3.3. Radiation Pattern Difference 36
Table 3.4. Simulation results from the optimisation assessment 37
Table 4.1. PWD for each body part 49
Table 4.2. Path loss for each simulated radio link and distance between antennas. 51
Table 4.3. PWD of measured radiation patterns on the chest. 54
Table 4.4. Approximated radio channel distances for each individual and body posture. 56
Table 4.5. QLOS and NLOS on-body paths 57
Table 4.6. Simulations and measurements path loss comparison 60

List of Acronyms

ABC	Absorbing Boundary Conditions
AoA	Angle of Arrival
BAN	Body Area Network
CM	Channel Model
DT	Diffraction Theory
ECG	Electrocardiogram
EEG	Electroencephalography
EMG	Endoscope and Electromyography
FDTD	Finite-Difference Time-Domain
FEM	Finite Element Method
FIT	Finite Integration Technique
GO	Geometric Optics
GSM	Global System for Mobile Communications
GTD	Geometrical Theory of Diffraction
ICNIRP	International Commission on Non-Ionizing Radiation Protection
IEEE	Institute of Electric and Electronics Engineers
IM	Image Method
ISI	Inter-Symbolic Interference
IT	Institute of Telecommunications
LAN	Local Area Network
LOS	Line of Sight
LW	Lines per Wavelength
MGE	Maxwell's Grid Equations
MoM	Method of Moments
NFDTD	Nonorthogonal Finite-Difference Time-Domain
NLOS	Non Line of Sight
PAD	Pattern Average Difference
PAN	Private Area Network
PWD	Pattern Weighted Difference
PDP	Power Delay Profile
QLOS	Quasi Line Of Sight
QoS	Quality of Service
RL	Mesh Line Ratio Limit
RT	Ray Tracing

SAR	Specific Absorption Rate
SBR	Shooting and Bouncing Rays
UMTS	Universal Mobile Telecommunications System
UTD	Uniform Theory of Diffraction
WLAN	Wireless Local Area Network

List of Symbols

α_{-3dB}	Half power beam width
δ_{AD}	Pattern average difference
δ_{WD}	Pattern weighted difference
ε	Electric permittivity
ε_0	Electric permittivity in vacuum
ε_1	Electric permittivity in dielectric 1
ε_2	Electric permittivity in dielectric 2
ε_{pmn}	Radiation pattern relative difference in each position
ε_r	Relative electric permittivity
$\sqrt{\varepsilon_{rM}}$	Maximum refractive index
$\sqrt{\varepsilon_{rm}}$	Minimum refractive index
η_{eff}	Radiation efficiency
θ_n	Azimuthal angle
λ	Wavelength
μ	Magnetic permeability
μ_0	Magnetic permeability in vacuum
μ_r	Relative magnetic permeability
ρ	Electric charge volume density
σ	Conductivity
φ_m	Polar angle
$\bar{a}$	Mean value
a_i	Simulation time sample
b	Magnetic flux
$\mathbf{B}$	Magnetic induction field
c	Speed of light in vacuum
$\mathbf{C}$	Discrete curl operator
$\tilde{\mathbf{C}}$	Dual discrete curl operator
d	Electric flux
$\mathbf{D}$	Electric displacement field
$d\mathbf{A}$	Differential vector element of surface area A, with infinitesimal small magnitude and direction normal to surface S
$d\mathbf{s}$	Differential vector element of path length tangential to the curve
$d\mathbf{V}$	Infinitesimal differential element of volume V

e	Electric voltage
$\mathbf{E}$	Electric field
E_{1t}	Tangent component of the electric field in dielectric 1
E_{2t}	Tangent component of the electric field in dielectric 2
E_{1n}	Normal component of the electric field in dielectric 1
E_{2n}	Normal component of the electric field in dielectric 2
f_r	Resonance frequency
G	Radiation pattern value
G_{IEEE}	Antenna gain
G_{ref}	Reference radiation pattern value
h	Magnetic voltage
$\mathbf{H}$	Magnetic field
j	Electric flux density
$\mathbf{J}$	Current density
j_s	Surface electric flux density
$\mathbf{J_S}$	Surface current density
K	Number of samples
l	Length
L_P	Path loss
M	Total number of increments in the polar angle
$\mathbf{M_\varepsilon}$	Electric permittivity coefficients matrix
$\mathbf{M_\mu}$	Magnetic permeability coefficients matrix
$\mathbf{M_\sigma}$	Conductivity coefficients matrix
n	θ Increment of 1º
N	Total number of increments in the azimuthal angle
P_e	Power fed to the transmitting antenna
P_r	Power available at the receiving antenna
q	Electric charge
s_K	Standard deviation
$\mathbf{S}$	Discrete divergence operator
$\tilde{\mathbf{S}}$	Dual discrete divergence operator
S_{11}	Antenna reflection coefficient
v_{emw}	Velocity of an electromagnetic wave

List of Software

CST Microwave Studio	This tool is specialist for fast and accurate 3D Electromagnetic simulation of high frequency problems. It has a broad application range and offers substantial advantages, such as shorter development cycles, virtual prototyping before physical trials and optimisation instead of experimentation.

Chapter 1

Introduction

This chapter gives a brief overview of the work. The application environments in which this MsC Thesis falls are briefly referred, as well as, simulation and measurement methods. The standard for this new type of technology is also quoted.

1.1 Overview

Technology has advanced far beyond what would be expected just a few years ago. Constant developments in electronics miniaturisation, telecommunications, simulation techniques, allied to the mankind perpetual search of well-being, have made room for the appearance of body-centric communications networks where small and light weighted equipment can be used on the body's surface, inside it, attached to vests or used in pockets.

The appearance of BANs and PANs comes from many and different today's necessities. The global network in which we live today, associated to these body-centric networks, allows anyone to be anywhere, while connected to everyone and everything, making the range of these networks appliance to be only limited by imagination and necessity. Applications within these types of networks have the main objective of improving directly and indirectly the life quality of those who wear it, whether at the professional or leisure level. When the maximum range of the network is touch, it called a BAN and it is a PAN when the maximum range is about 10 m.

Some application environments, among others, are:

- Professional Activity– In space, sensors will help in a better understanding of how living systems respond to the impact of microgravity and spaceflight. This can be achieved either with sensors that measure temperature, heart rate, blood pressure and any other relevant physiological parameters. In the military context, sensors are targeted to support military personal in battlefields, as an example, a smart shirt with integrated sensors and optical fibbers, which detects bullet wounds and monitors body's vital signs such as heart rate and body temperature is under development by Institute of Electrical and Electronics Engineers (IEEE). For militaries, other possible applications are wearable antennas that can be perfectly dissimulated in the clothes, with the purpose of communicating to mid range or long distances, to another platoon in the field to know its situation, or to receive orders and give mission reports to a higher rank. The antenna must be dissimulated because the responsible soldier for the communications is the first shooting target of any enemy, and with an antenna like this one he would easily blend among the others.
- Medical – in this context, sensors can be used either in hospitals as in smart homes. They can help patients having remote care giving and detection of early signs of disease, in order to monitor those conditions in patients a wide variety of body sensors are required, as well as, the capacity of wireless communication between them. Depending on whether sensors are implanted inside the body or in close proximity it, there are different possible applications. Vital data about humans, such as heart rate, Electrocardiogram (ECG), Electroencephalography (EEG), among others will be possible to perform a hospital, as well as, home and outdoor environments. In outdoors or at homes, it will be possible because the bedside monitor can be replaced by a data collection device, which records the information, or a gateway implemented

by a cell phone that communicates to a central database, resulting in much fewer mobility restrictions. Artificial organs are also a possible application, limbs for example, which have to be in constant movement, can be controlled by manual controllers, thoughts or external devices. Besides moving some kind of artificial organs, it might also be necessary to monitor and control them as well as any other implants, being necessary to transmit their data.

- Fitness monitoring - applications referred above are mainly to save lives, in addition, it is also possible to use this technology to many other things, such as fitness monitoring through the gathering and display of relevant data to the exercise. Measuring heart rate is already used worldwide, but in order to have a more beneficial exercise session much more information is helpful, such as body temperature, oxygen level, and location information [HaHa06a].
- Leisure – in music reproduction, for example, this technology can also have application. Supposing someone is listening to music on his personal music player and then he receives a call from the mobile phone. One possible application scenario would be a wireless headset that mutes the music and answers the call. After terminating the call the headset restarts music playback.

Mobile communication devices will have an important role, because they will allow data transmission between PANs and/or BANs with the outside world, such as the mainframe that keeps the information, the doctor responsible for a certain patient or even to call an emergency team. The system used to communicate depends on the specific implementation, and it can be a WLAN or cellular one (e.g., GSM or UMTS). This device would be the central point to which all terminals would connect, managing them. Fig 1.1 depicts one possible case scenario of all these internetwork connections, where BAN is used for fitness monitoring.

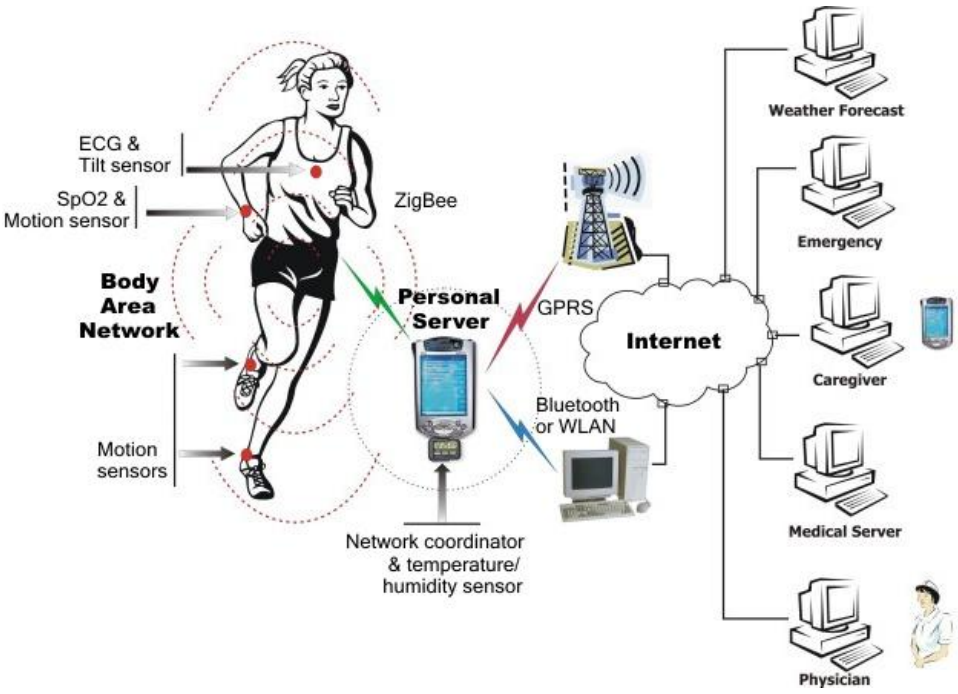

Fig 1.1. Representation of a BAN and all the backbone with which the BAN may be connected. (extracted from [Wica10])

In order to be user friendly, communications between devices, on BANs and/or PANs, must be wireless, causing channel issues due to body's geometry and reflections on the surrounding environment. With this, in body-centric communications comes the necessity to make simulations and measurements in order to evaluate the interaction between electromagnetic waves and body. Properties of body tissues, such as conductivity (σ) and relative permittivity (ε_r) vary greatly with frequency and tissue type. In order to make measurements without using human live tissue, phantoms were invented. Phantoms can be simulated biological bodies or physical models simulating biological tissues characteristics within a certain frequency band.

When simulating, many numerical modelling techniques can be used, depending on the situation. The innovation introduced in this MsC Thesis has to do with the use of FIT, which is the method used by *CST Studio Suite 2010*, as the chosen numerical method to simulate the influence of the human body in a radio channel, and comparing it with the measured data of the used antenna [MeCa06]. In our specific study environment, the human body and close distances to it, there are many boundary-value problems and one of the best numerical methods to solve those problems is the FIT Method.

Yee proposed Finite-Difference Time-Domain (FDTD) in 1966 [YeeK96], but it became only widely known in 1972, when Prof. Allen Taflove was trying to obtain a model for UHF and microwave penetration into the human eye in order to better understand the formation of "microwave cataracts". The problem was that the existing methods were just capable of solving only some hundreds of field unknowns and the eye geometry required the solution of something like 100,000 field unknowns. He ended up discovering Kane Yee's 1966 paper. Yee algorithm could deal with material inhomogeneities and did not require matrix inversion, facilitating the solution of the problem. In 1977, Weiland introduced a distinct numerical method, in which the main difference from FDTD is that it uses the Maxwell's equations but in the integral form.

Much work had already been developed, but there is still much to do. Due to advances in wireless technology, new types of Wireless Local Area Networks (WLAN) were developed. IEEE has developed a standard called IEEE802.15.6 (Body Area Network) where the task group TG6 is responsible to develop in-body and on-body devices for medical and non-medical purposes [YaSa09], however it can also be used some of the existent technologies, for example ZigBee IEEE802.15.4 as depicted in Fig. 1.1. The task group TG6 standardized the relation between frequency band and the scenario of each possible antenna radio link, as depicted in Table 2.1. The frequency bands which are being used, belong all to the Industrial, Scientific and Medical (ISM) bands.

It must also be taken into account that these systems are to be used in movement, in everyday activities. That is why tests have already been made in order to estimate the influence of different body postures regarding the signal received with antennas around the body.

Advancements in antennas are also notorious in utilizing antenna substrates made of textile materials. These types of antennas will make possible the existence of smart clothes because they are malleable and the communication between sensors will be wireless, making it much more user friendly.

Communication mechanisms between antennas will depend on the positioning of the antennas and

the transmission channel. The wave will always follow the easiest path and it can be free space propagation, through diffraction having the body as an obstacle or a creeping wave on the body's surface.

Body-worn equipment is certainly a future trend because it will increase the quality of life of those who wear it. At the moment the existing equipment is still very heavy and wires make the connection between modules, but in the future they will be lighter and wireless.

This thesis is composed by 5 chapters as main body and an appendix formed by 3 annexes, identified from 1 to 3. The thesis has the following structure:

- In chapter 2, it is given the description of body-centric communications regarding categories, already standardized frequency bands and applications. This chapter also address the human body characterization and modelling, discussing dielectric properties of the materials, as well as, numerical and physical representations of the human body. Some modelling techniques are also depicted, briefly discussing FIT and errors associated with this particular modelling technique, due to its importance in this work. This chapter discusses some propagation mechanisms on the body surface and inside it, as well as, some antennas already developed and its most suitable use.
- In Chapter 3, is depicted the problem under study in this work followed by a detailed description of the simulation tool used, as well as, FIT modelling technique. It is also presented the results from a resolution assessment and its objectives to the realisation of this work.
- In Chapter 4, the scenario set in this work is presented, as well as, the results from the simulations and the measurements concerning radiation patterns, antenna characteristics and radio channel characterization. In the end of this chapter, the results are compared.
- In chapter 5, the most relevant conclusions, future research topics and personal opinions are presented.

Chapter 2

Body-centric Communications

This chapter provides an overview of the communication systems in the vicinity of a human body, concerning both antennas and body issues.

2.1 Body-centric communications and frequency bands

2.1.1 Body-centric communications categories

The current technological evolution made possible the appearance of devices with smaller dimensions and longer battery autonomy, making room for the existence of new types of Local Area Networks (LANs) centred on the human body, namely PANs and BANs. In BANs, communications are done between on-body and/or in-body systems. In PANs, communication is done between an on-body device and other devices in an area with about 10 m radius. These other devices can be connected through GSM or other wireless systems to points of care where data can be given a proper use, as depicts Fig. 2.1.

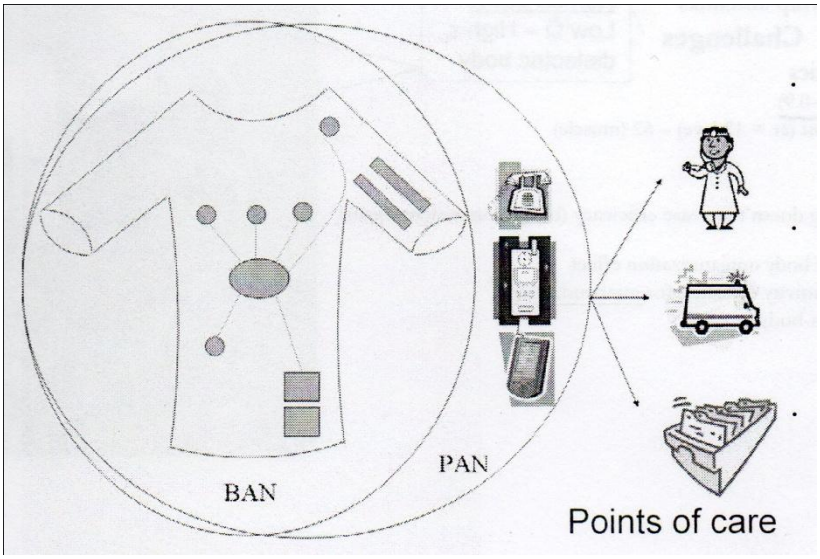

Fig 2.1. Representation of the influence area of a BAN, a PAN and points of care (extracted from [HaoY09])

Depending on the data collected and the use that it will have, there are different types of body-centric communications within the sphere of BANs and PANs:

- Off-body – communications are established between an on-body and an off-body device or system.
- On-body – components of on-body networks and wearable systems that communicate with each other.
- In-body – implants communicate with other implants or on-body sensors.

This type of classification implies the division of the region that includes booth PAN and BAN areas into 3 different zones. The first domain is where the most of the channel is off the body and in the surrounding area, approximately 10 m, having just one antenna of the link on the body's surface. Communication between localised base stations or broadcast stations with transceivers located on the body, have been studied extensively in [FaAg00], [Stra03] and [Schw02]. These investigations include studies of the propagation characteristics in urban and rural environments, as well as, studies of the performance of body-worn antennas with variations of the body proximity and orientation.

The second domain is where the communicating antennas are disposed on the body and the most of the propagation channel is also on the body. Nowadays, the main problem is the fact that many systems are wired, causing reliability issues due to cables and connectors bending as well as the weight that is inconvenient to the user [HaHA06a]. Other connection methods are under study, such as smart textiles and using the human body as a communication channel, but besides the advantages, they also have negative aspects, for example, smart clothes using wearable antennas need a special garment to be worn, which may go against user's personal preferences, while using the body as a communication channel have a very low capacity due to tissue absorption [HaHa06]. It is obvious that wireless radio connectivity is the future for connecting on-body devices, but there are three main criteria that communication between modules must meet in order to be successful, support the high data rates to enable many applications including video, be small and lightweight in order to be user friendly and have power efficient links in order to enable a longer autonomy.

The third domain has a great portion of the channel inside the body, and implanted transceivers are used i.e., the in-body domain. Nowadays, there are a number of situations where implants improve widely patient life quality, such as pacemakers [Perr93], and cochlea implants [Loiz98].

Healthy Aims [Heal10] has projects in this domain, related with incorporating pressure sensing in the brain cavity, glaucoma sensors and retinal implants. Other future aims are the lab-on-a-chip for internal diagnosis, interfacing to nerve endings for communications to the brain [Ming03] and automatic drug delivery [Fige00].

2.1.2 Systems frequency bands and applications

Depending on the application, a certain bit rate and a consequent frequency band is required, e.g., if the objective is only to measure and transmit heart rate it just needs a small band, but if allied to that is also necessary to measure, for example, the oxygen level, the body temperature, the sugar level and measure the distance run during a training, the necessary bit rate will greatly increase.

IEEE has organised a Task Group, called TG6, responsible for developing a standard for BANs, named IEEE802.15.6 [YaSa09], for medical and non-medical devices that could be placed in and on the body. A list of scenarios, in which IEEE802.15.6 will be functioning, can be identified. These scenarios along with their description and frequency band are listed in Table 2.1. Based on the location of the communication nodes, i.e., implant, body surface and external, scenarios are named. The scenarios are grouped into classes that can be represented by the same Channel Models (CM). From what was said in Sub Section 2.1.1, CM1 and CM2 represent in-body communications with exception to S3 which can be considered as a combination of scenarios S2 and S6 or S7, CM3 and CM4 corresponds to on-body and off-body communications, respectively.

Nowadays, there are already a large number of applications, and in the future they will certainly be many more. Depending on whether sensors are implanted inside the body or in close proximity to it, there are different possible applications, some examples are presented in [Reic09]. Vital data about humans, such as heart rate, Electrocardiogram (ECG), Electroencephalography (EEG), among others,

are normally associated with low data rate applications, these applications' environments will be the hospital, as well as home and outdoor environments. Even outdoor or at home will be possible because the bedside monitor can be replaced by a data collection device that records the information or a gateway, implemented for example by a cell phone that communicate to a central database, which will be a great leap in patient monitoring, because they will have much less mobility restrictions. BAN medical applications can be grouped into three different categories, depending on the amount of traffic they generate and the Quality of Service (QoS) required: best-effort low data rate for routine actions such as supervision and control, real time low data rate for ECG and heart rate among others, and real time high data rate for Endoscope and Electromyography (EMG). When dealing with life systems, there are always very rigorous requests on medical signals in terms of accuracy, reliability and latency. In a worst case scenario, it is required less than 10 Kbit/s per sensor for vital data. Assuming that any BAN and medical application will have no more than 20 sensors and including the network overhead, the total traffic is less than 500 kbit/s [HaHa06a].

In what concerns in-body communications, it is worthwhile referring artificial organs, which might have to be in movement, such as limbs for example, which can be controlled by manual controllers, thoughts or external devices. Besides moving some kind of artificial organs, it might also be necessary to monitor and control them as well as any other implants, and it may be necessary to transmit their data.

In this context, there will be wearable sensors that are targeted to some risk professions, such as military personal in battlefields, fire fighters and astronauts. A smart shirt with integrated sensors and optical fibers is under development, which shirt detects bullet wounds and monitors the body's vital signs, such as heart rate, body temperature among others.

The applications referred above are mainly to save lives. In addition, it is also possible to use this technology to many other things, such as fitness monitoring through the gathering and display of relevant data to the exercise. Measuring heart rate is already used worldwide, but in order to have a more beneficial exercise session much more information is helpful, such as body temperature, oxygen level, and location information [HaHa06a].

In what concerns music reproduction this technology can also be applied. Supposing someone is listening to music on his personal music player and then he receives a call from the mobile phone. One possible application scenario would be a wireless headset that mutes the music and answers the call. After terminating the call the headset restarts music playback. Assuming that only compressed audio is exchanged between devices, data rates, in this case, are within 500 kbit/s.

Mobile communication devices will have an important role, because they will allow data transmission between PANs and/or BANs with the outside world, such as the mainframe that keeps the information, the doctor responsible for a certain patient or even to call an emergency team. The system used to communicate depends on the specific implementation, and it can be a WLAN or cellular one (e.g., GSM or UMTS). This device would be the central point to which all terminals would connect, managing them. Excluding business applications that might need a capacity of some Mbit/s, but normal network scenarios should stay below 500 kbit/s. In Table 2.1 all the possible scenarios are

shown, taking into account if there is Line of Sight (LOS) or Non Line of Sight (NLOS).

Table 2.1. List of all possible scenarios and their descriptions (extracted from [YaSa09])

Scenario	Description	Frequency Band [MHz]	Channel Model
S1	Implant to implant	[402,405]	CM1
S2	Implant to body surface	[402,405]	CM2
S3	Implant to external	[402,405]	CM2
S4	Body surface to body surface (LOS)	13.5, 50, 400, 600, 900, 2400, [3100,10600]	CM3
S5	Body surface to body surface (NLOS)	13.5, 50, 400, 600, 900, 2400, [3100,10600]	CM3
S6	Body surface to external (LOS)	900, 2400, [3100,10600]	CM4
S7	Body surface to external (NLOS)	900, 2400, [3100,10600]	CM4

2.2 Human body characterisation and modelling

2.2.1 Dielectric properties

Determining the dielectric parameters of body tissue is very difficult because it is difficult to obtain samples and making measurements in live tissue is impossible because the measuring device must be in contact with the tissue. Usually, measurements are only done in freshly killed sheep and in human autopsy materials. Depending on the frequency band used in an application, dielectric properties of tissues will vary as well as penetration depth, as can be seen in Fig. A1.1, Fig. A1.2 and Fig. A1.3. Muscle and fat are the two types of tissues that fulfil the major part of our body, making them the most important to study.

Differences are notorious in conductivity and relative permittivity across a wide range of frequencies for these two tissues, but between approximately 300 MHz and 2.9 GHz variations are small. Fat at 300 MHz has a relative permittivity of 5.6, and at 2.9 GHz its value is 5.2, in what concerns conductivity, it takes values 0.04 $S.m^{-1}$ and 0.13 $S.m^{-1}$, for 300 MHz and 2.9 GHz, respectively. Muscle's conductivity varies between 0.77 $S.m^{-1}$ and 2.10 $S.m^{-1}$, and the relative permittivity varies between 58.4 and 52.2, for the same frequency band as fat.

Age also makes dielectric properties vary due to the percentage of water in tissues.

Another important issue to take into account is that the penetration depth decreases as the frequency increases. At 100 MHz, penetration depths are 400 mm and 70 mm for fat and muscle respectively and thus this frequencies are used to communicate with medical implants and in-body sensors, whilst

at 2.45 GHz penetration depths are 113 mm and 21 mm also for fat and muscle which make propagation take place around the body surface.

Another thing that must be referred is the dielectric boundary conditions, since the environments under study will be air and body tissues.

Suppose an interface between two different dielectric regions, each one with a respective permittivity $\boldsymbol{\varepsilon_1}$ and $\boldsymbol{\varepsilon_2}$. There will exist in each region, different electric fields **E** and in order to relate those fields it is necessary to assure the dielectric boundary conditions.

Both **E** fields can be decomposed in terms of tangential and normal components taking as reference the boundary between the dielectrics. It is important to refer that boundary conditions just give information about the relation between the vector fields only in the dielectrics interface. Inside each dielectric there is not any information that can be obtained directly from these statements [JimS04]).

The tangential boundary condition can be written as:

$$E_{1t}=E_{2t} \quad (2.1)$$

and the normal boundary condition is:

$$\varepsilon_1 E_{1n}=\varepsilon_2 E_{2n} \quad (2.2)$$

where:

- E_{1t}: tangent component of the electric field in dielectric 1
- E_{2t}: tangent component of the electric field in dielectric 2
- E_{1n}: normal component of the electric field in dielectric 1
- E_{2n}: normal component of the electric field in dielectric 2
- ε_1: electric permittivity in dielectric 1
- ε_2: electric permittivity in dielectric 2

2.2.2 Phantoms

There are two main types of phantoms, physical phantoms that simulate the characteristics of the biological tissues within a certain bandwidth, and numerical phantoms that simulate biological tissues to use in computational simulations and theoretical analyses.

Physical phantoms have extreme importance in BAN's development, because they are the only way to make experimental measurements related with the interaction between human body and electromagnetic fields. Diverse safety rules, such as those defined by IEEE [IEEE03] and International Commission on Non-Ionizing Radiation Protection (ICNIRP) [ICNI98], set radiation tolerable levels in terms of Specific Absorption Rate (SAR), which are impossible to define without the measurements performed in phantoms.

Phantoms are also an asset to study radio wave propagation in and on the body, in order to design good quality wearable communication devices. They can be classified as solid (dry), semisolid (gel), solid (wet) and liquid.

Solid (dry) phantoms are a good option when it is necessary to measure the SAR in body's surface, or

when developing a well-defined internal structure with several organs with different dielectric characteristics. Some proposed types of phantoms are composed by:

- A mixture of ceramic and graphite powder [Tamu97].
- Silicone rubber mixed with carbon fibber [NiKi96].
- Conductive plastic containing carbon black [Chan00].

Solid (dry) phantoms have the disadvantage that they need expensive equipment, as well as, special procedures in the composition production, such as, high temperatures and pressures. The other two types are easier to fabricate, but it can be difficult to produce large quantities of these materials.

Semisolid (gel) or solid (wet) phantoms possess a coagulant in order to self-shaping and eliminate phantoms' outer shell. A gel phantom was developed, being composed by water, TX-150 (polyamide resin), sodium chloride and polyethylene powder. These last two components are responsible for the control of conductivity and relative permittivity, respectively. These types of phantoms are mainly used to simulate organs with a high percentage of water such as brain and muscle. Another type of solid gel phantom has in its constitution polyacrylamide, which is a very toxic material, and because of that special care is needed. The great advantage of this substance is the fact that it simulates equally materials with a high and low percentage of water, however it degrades over time due to water loss and/or fungi growth.

Liquid phantoms are the oldest phantom types, and basically consist in a container filled with a liquid that, within a certain frequency bandwidth, have the same dielectric properties has the tissues in the human body. These phantoms are used in SAR studies, measuring in a very accurate way the distribution of the electric fields inside the phantom with a probe. It is easy to see that this kind of phantom characterises, in a very inaccurate way, the human body because the phantom is filled up with a homogenous medium. This type of phantom also has a very narrow band in which dielectric properties are equal to human tissues, besides that, it is difficult to handle the container in the test environment and the container dielectric characteristics are also difficult to set. Despite these inconvenient, it has the advantage of being easy to fabricate.

Phantoms can vary from complete bodies in a specific position or just a part of it, such as a head, a torso, an arm and any other part that is required depending on the objective of the research.

In simulations, generally are used simple-shaped phantoms and they go by the name of theoretical phantoms. When it is required to use a more realistic numerical phantom it is used a voxel phantom.

Theoretical phantoms can be homogeneous or layered flat phantoms if, for example, it is necessary to evaluate EM dosage. Spherical models are used for EM dosage in human head and eyes, while cylindrical are used for whole body models as well as arms.

Voxel phantoms, as depicted in Fig. 2.2, are composed by small cubes (voxels), each one of those voxels can be programmed to have different dielectric properties so they can simulate different organs, in order to be the closest possible to a real human body. With this kind of phantom it can also be simulated for example children, as well as pregnant women, which is impossible with physical phantoms due to security issues.

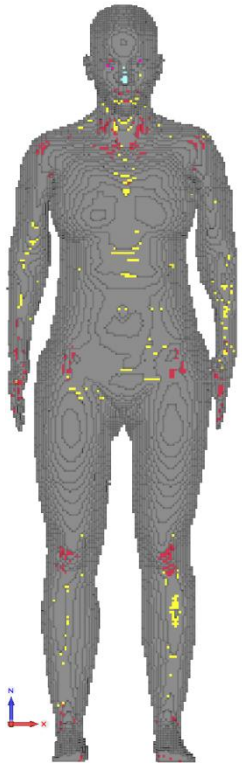

Fig 2.2. High-resolution female whole-body human voxel model (extracted from [CSTM10]).

2.3 Numerical modelling techniques

2.3.1 Modelling techniques

Since antennas started being used near the body, the need for numerical modelling of human body arose. In the beginning it was used to calculate the SAR, due to mobile phones and the shadowing effect for wireless networks in indoor environments, however with technological evolution new appliances for numerical modelling of on-body antennas emerged at high frequencies, mainly in the area of microwaves. Here, the human body guides surface waves and reflects space waves. The need for simulation arise from the fact that when more than two communication nodes are on the body or very close to it, changes occur in the polarisations, orientations of the antennas and propagation path length due to different body postures, causing additional loses and variations in path gain.

In on-body communication systems, the dimensions of the body are large compared to the wavelength used, allowing the approximation of the human body as a homogenous dielectric with high attenuation. Several numerical modelling techniques are used to analyse electromagnetic problems in the area of body-centric wireless communications [Tafl95].

The Uniform Geometrical Theory of Diffraction (UTD) and its previous version, the Geometrical Theory of Diffraction (GTD) are based, as the name indicates, on Geometric Optics (GO) and Diffraction

Theory (DT) [Kell92]. This numerical method assumes that all waves are plane, in order to use Ray Tracing (RT). Reflection and transmission are interactions between propagation waves and the surrounding environment, which depends on the polarisation of incidence and can be calculated by classic formulations. Wedge and corner diffraction are forms of scattering by objects, whose size is of the same order of magnitude as the wavelength. Diffraction accounting in UTD modelling is fundamental as in any other modelling technique, because otherwise abrupt changes in field strength would occur if the receiver moves from LOS to NLOS conditions. Creeping wave is also a kind of diffraction that is different from GO and consists in a ray tangential to curved surfaces that moves along it.

RT techniques are used to characterise wireless communication systems (e.g., WLAN, mobile phones, personal communication systems) with respect to site-specific prediction. This technique is extensively used to predict indoor radio propagation, which is an environment with multipath reception conditions, providing data such as Angle of Arrival (AoA) and Power Delay Profiles (PDP). RT has two different models: the Image Method (IM) and the method of Shooting and Bouncing Rays (SBR). The IM is used to analyse radio propagation in an environment with low geometrical complexity and few reflections, whilst SBR method generates an amount of rays that may or may not reach the receiver. In the SBR method, refraction and diffraction phenomena can be considered, if necessary, for the problem resolution.

Another technique that must be referred is the Method of Moments (MoM), which is used to transform complex integral equations into a system of simple linear equations, through the use of weighted residuals technique [Harr68]. This method can be used either in time and frequency domains, being used preferentially to simulate thin-wire structures rather than objects with varying dielectric properties or complex geometries.

The Finite Element Method (FEM) has in its main idea the division of the electromagnetic structures with curved boundaries into several shapes such as rectangular or triangular. The most important disadvantage of this method is that it is very time consuming to get a solution, because the computational complexity is the highest among all existing methods. FEM has been applied mostly for medical applications at low MHz frequencies due to computer memory restrictions.

Combining both MoM and FEM simulations can be made, for example, for SAR calculations where MoM can be used, for example, to model the metallic surfaces and wires of the base station antenna, and FEM to model human phantom heterogeneous.

FDTD method, as well as FEM, divides structures under study into small cells making it appropriate for modelling inhomogeneous media and complicated boundaries.

FDTD requires only $O(N)$ computer complexity, whilst MoM and FEM have need of $O(N^2)$, where N represents the number of unknowns. Besides its usefulness and positive points, as any other numerical technique, this one has its own frailties. It requires the entire computational domain to be meshed and these cells must be small compared to the used wavelength (about 10 to 20 times smaller) and to the smallest element to model [HaHa06a]. This will make it difficult to model thin and

long structures as well as structures that are curved because the edges will be stair-cased. When configurations have sharp edges it will be required a very small grid size resulting in a small time step.

FDTD is a method to solve directly Maxwell's time dependent curl equations and do not demand the use of potentials. Instead, it is based in volumetric sampling of the zone within and surrounding the element under study, over a period of time of the unknown electromagnetic near-field distribution (**E** and **H).** This method has two types of sampling, in time to ensure numerical stability of the algorithm, and in space where is necessary a resolution with about 10 to 20 samples per wavelength, as referred before [Tafl95].

On the whole, FDTD simulates electromagnetic waves in a well-defined restricted spatial region during a period of time divided into time-steps. If the modelled region is considered infinite than Absorbing Boundary Conditions (ABC) are put to use at the external grid truncation planes, in order to permit all leaving signals to exit the region without reflecting.

Phenomena as for example scattering and multiple scattering, induction of surface currents, aperture penetration and cavity excitation are calculated time-step by time-step through numerical analogue to the curl equations [Tafl95].

Reliability of these phenomena values is guaranteed if their spatial and temporal variations are well explained by the space and time sampling process. The expected result is a self-consistent model with the coupling of all the small cells that compose the structure under study independently of its total size [Tafl95].

FDTD can be divided into three different classes that do not depend on how the solvers work, but in how the space grid is defined.

In *almost completely structured* gridding method, a Nonorthogonal FDTD (NFDTD) algorithm is used, in which the grid is structured so that its volumetric cells are congruent whenever possible. In this case, supposing cubic cells and that the object being modelled is a human body, the result is a staircase model that is, as close as possible, equal to the original surface. However work has already been conducted in order to solve this problem and that was accomplished modifying the size and shape of surface cells as can be seen in [JuTa92].

As the structures increase their size, more efficient this method becomes because the number of modified cells is proportional to surface. This modified cells become a smaller percentage as the structure increases and the computational requirements to implement the full model are mainly needed for the stepped-surface model. As a disadvantage, this method needs the construction of specific geometry-generation software.

Another method is the *surface-fitted* one*,* and in this case the space grid is totally deformed, in order to adjust the structure to the model. Unlike the previous method this one already have grid generation software for this kind of situations, but it needs more memory allocation for the position and distortion factors of each voxel, and extra computer arithmetic operations to implement Maxwell's equations at each cell and to implement field stability between cells boundary.

The third and last method is called *completely unstructured*, and in this case the structure under study is composed by cells with several sizes and shapes, so that the structure surface remains equal to the original. Similarly to the previous case, there is available software to model structures with this method, unfortunately its irregular assembling requires a robust pre-processing algorithm that allocates each type of cell composing the structure to a specific processor.

In any type of wireless system it is necessary to optimize the location of nodes in order to warrant suitable system coverage. In body-centric wireless systems is even more important and difficult because of body's movement. RT and FDTD methods have been used to establish many statistical and site-specific models for narrowband indoor/outdoor propagation analysis.

In what concerns Yee's algorithm, it solves the **E** and **H** fields in space and time using the coupled Maxwell's curl equations in lieu of solving **E** and **H** field alone. This makes the solution more reliable for a wider class of structures. Yee's algorithm also centres **E** and **H** components in a three-dimensional space to that each **E** component is surrounded by four circulating **H** components and each **H** component is surrounded by four circulating **E** components.

In the time domain Yee's algorithm also centres both electric **E** and **H** components in time in a way called *leapfrog* arrangement, as shown in Fig. 2.3. For a certain time instant, **E** calculations in the space of interest are finished and stored using the **H** data, recorded in the previous time step. Than all of the **H** calculations are executed and stored using the **E** data just computed, after this the cycle is repeated until time-stepping conclusion. This method avoids problems with matrix inversions and simultaneous equations. In time domain as well as space domain the finite-difference expressions used in the Maxwell's curl equations are central in nature and second-order accurate [Tafl95].

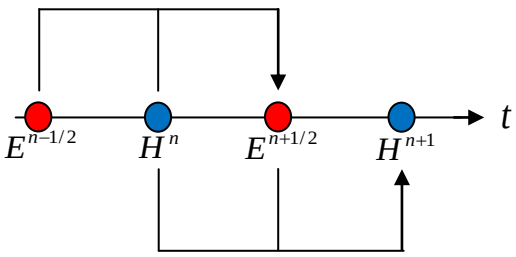

Fig 2.3. Representation of the leapfrog arrangement (extracted from [CSTH10]).

Like FDTD, The FIT stands out due to high flexibility in geometric modelling and boundary handling, being the reason why it is the method used in *CST Studio Suite 2010*. Anisotropy, non-linearity and dispersion are material properties that FIT can incorporate.

This method is specially suited for transient field analysis in RF applications because it uses the leapfrog explicit time integration scheme together with a Cartesian grid. This leads to extremely robust algorithms with low calculation time and memory requirements.

While FDTD uses Maxwell's Differential Equations, FIT uses the Integral Equations. This method consists in a universal spatial discretisation in order to solve numerically, electromagnetic field problems, both in time and for a wide range of frequencies. This method will be addressed in more

detail further in Section 3.2.

2.3.2 Error Sources

All discretization methods introduce errors, either because the model is not a perfect duplicate of the real model or because the numerical simulation is subject to errors itself. Many of these errors can be negligible in practice, but it is necessary to know their existence, in order to make sure that the results are reliable [CSTM10].

In what concerns differences between the numerical model and the real model, some sources of errors can be recognized.

Geometric dimensions may be wrong, or geometric details may be neglected due to the resolution that the size of the cell offers. This can be avoided by comparing carefully both the drawing and the real structure. The influence of small details can be studied by carrying out the same simulation with and without details [CSTM10].

Material parameters may be wrong either because they are not exactly known or because the values possessed are not valid for the band of interest. It might be necessary, especially when investigating a broader band, to enter the correct frequency dependency of the material properties in order to obtain accurate results.

Sometimes the environment is not considered correctly, objects that are placed near the measured structure may influence the result and, in this case, should be included in the simulation model. If reflections are not to be considered, one possible way to overcome this difficulty is to realise the measurements in an anechoic chamber in order to have results with no errors introduced by reflections [CSTM10].

The simulation itself can also introduce error as is briefly referred when discussing FIT in Section 3.2.

To ensure accurate results, the electromagnetic fields need to be sampled sufficiently dense in space. The accuracy of the field solution increases with a finer mesh, and convergence is ensured by the FIT, diminishing the discretisation error but augmenting the computation time. The typical size of the mesh cells must be between 10 and 20 times smaller than the wavelength, in order to obtain a good compromise between calculation time and the achievable discretization error [HaHA06a]. Any meshing below 10 cells per wavelength gives very inaccurate values and any meshing above 20 cells per wavelength takes too much time for the accuracy that would be obtained.

It is important to take into account that the accuracy of the simulation tool is affected by all of these sources of error.

2.4 Antennas and propagation

2.4.1 Propagation Mechanisms

In ordinary mobile communications systems, the radio channel suffers fading due to interference between multi rays caused by scattering in the surrounding environment, whether outdoor or indoor. This fading that can just be characterised statistically, can cause losses of many tens of dB depending on the environment, and on-body systems communications are not an exception. However, in this situation it will also be necessary to account for the changes in the body's geometry. The human body is always moving even when standing or sitting, and this movement becomes much more important in radio channel characterisation when normal activities are performed or during practice of sports.

The position of the antennas on the body varies, depending on the application, as well as the geometry of the environment affecting the characterisation of wave propagation and the antennas' radiation pattern. On-body antennas will communicate through paths on the body and paths on the surrounding area, whether indoor or outdoor, due to reflections. In addition, during the channel characterisation phase, there are difficulties in working separately in antenna characteristics and in the propagation path because they are dependent. All these setbacks must be studied during the design of the transceivers, so that channel capacity and power consumption can be optimised [HaHa06b].

Path loss is the attenuation of an electromagnetic wave as it propagates through space, depending on the environment in which the radio channel is contained, different propagation models are used and consequent path loss will be obtained in a different way. These models are mainly empirical with equations based in measurements within a certain frequency band. For urban environments, for example, several models can be used depending on the situation, such as Okumura-Hata Model or Ikegami Model [HaHa06b].

On-body communication systems can also use human body as a transmission channel, constraining communications to touch and/or between on-body and in-body elements. As referred in Sub Section 2.2.1, in communications, with in-body elements, penetration depth will decrease as the frequency increases.

Some path loss measurements have already been conducted for on-body elements and some conclusions were taken. As quoted in [HaHa06b], some studies have been developed at 2.45GHz with the body in different positions, propagation paths can be with LOS or NLOS, in other words, transmitter and receiver can "see" each other or do not, respectively. Measured data showed that the LOS data follow the theoretical free space curve but with a mean difference between theoretical and measured data of about 5.1 dB. The used expression of the path loss in the illuminated region, with LOS, was:

$$L_{P[\mathrm{dB}]} = 5.33 + 20\log_{10}\left(l_{[\mathrm{cm}]}\right) \tag{2.3}$$

where:

- L_P : path loss
- l :length

The difference between the values given by the equation and the measured data in LOS as given a standard deviation of 4.2 dB and a possible reason for this value can be credited to the mutual orientation of the antennas.

Where the antennas do not have LOS the dominant propagation path will be throw diffraction or a creeping wave that propagates around the body. With this, the distance that the wave will have to make is unpredictable due to the human geometry in general, the position in which the body can be and anatomical differences between individuals. Howsoever experimental results seem to follow a trend that can be represented by the following expression:

$$L_{P[\mathrm{dB}]} = 0.36 \cdot d_{[\mathrm{cm}]} + 35 \tag{2.4}$$

In these test scenarios it is not possible to delineate a perfect boundary between LOS and NLOS and because of that there were situations in which the receiving antenna was in the frontier between the shadow and the illuminated region. This means that the slightest movement could make the antenna obstructed or unobstructed. Results showed that some data was clustered together with the NLOS while the rest follow the LOS trend.

The PDP is also a matter that needs much attention, in order to accurately determine maximum bit rates for an application. The same bit of a signal can arrive in different instants of time due to reflections and that can cause Inter-Symbolic Interference (ISI), resulting in a lower bit rate. In on-body communication systems, besides reflections in the surrounding environment, it must be also taken into account the fact that the signal might travel through different parts of the body reaching at different time instants.

The University of Birmingham conducted experiments in an anechoic environment and reached some conclusions about multipath on the body at 2.45 GHz. Two antennas were considered, one on the back as receiver and the other on the front, transmitting a wideband pulse. The experiment showed that strong signals were received coming from the shoulders, waist and from between the legs. Results were very similar to those obtained by measuring the physical length and calculating the propagation time.

Therefore, when talking about on-body communication systems, movement will have several consequences that will affect the radio channel. The experiences above were made with static bodies but it have been said that the objective of BANs is to guaranty total mobility to the user. When doing tests with moving subjects, one possible characterisation for on-body links can be done taking into account the parts of the body where the antennas are (e.g., trunk-to-trunk, trunk-to-head, trunk-to-limb), because each one of them have different intensities of movement. It is easy to see for example that trunk-to-limb connections will have more fluctuations than trunk-to-trunk and because of that, propagation channel characteristics are expected to be different for each case, due to link geometry variability, so, when developing new equipments, all this possibilities must be taken into account. In Fig. 2.5 it can be seen two belt-to-chest path loss, one between two monopoles and the other between

a monopole and a disc monopole. The measurements represented in Fig 2.4 take place with the body in each posture during 20 s. The body postures were the following: 0-20 standing; 20-40 standing, body turned left; 40-60 standing, body turned right; 60-80 standing, body bent forward; 80-100 standing, head bent forward; 100-120 standing, head turned left; 120-140 standing, head turned right; 140-160 standing, arms stretched out to side; 160-180 standing, arms above head; 180-200 standing, arms forward; 200-220 standing, forearms forward; 220-240 standing in an arbitrary position; 240-260 sitting, arms hanging; 260-280 sitting, hands on lap; 280-300 sitting in an arbitrary position; 300-320 standing; 320-340 walking, arms close to body; 340-360 walking, arms swinging free [HaHa06a].

Another aspect that must not be overlooked is reflection. The anechoic chamber is used in tests to avoid any reflections in walls or any other object, but in normal environments that happens and have an effect that must be taken into account in the link budget. Depending on the frequency used, and in the total distance that the reflected signal has to travel, the sum of the two signals can be constructive or destructive.

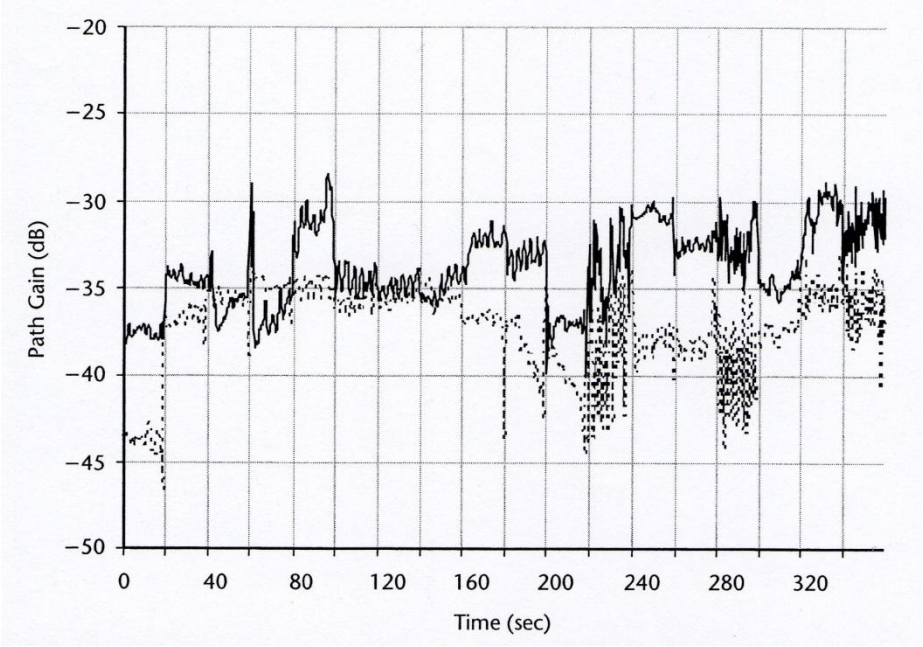

Fig 2.4. Measured belt-to-chest path gain with monopole to disc monopole antennas (solid line) and monopole to monopole antennas (dotted line) at 2.45 GHz (extracted from [HaHa06a]).

2.4.2 Antennas

In a type of environment near, in or on a body, antennas need to meet, the best possible, special requirements, such as, be insensitive to the proximity of the body and must have a radiation pattern shape that minimizes the link loss. Measurements showed that path gain is highly dependent on antenna type and link geometry.

Antennas positioning is also very important because it will determine the propagation mode, for example, in a situation with a belt-to-chest path, it is easy to see that it will exist a creeping wave on the body's surface. In this case the antenna needs to have a radiation pattern peak along the body

surface [HaHa06a].

Supposing a belt-to-wrist path, it can either exists a free space path or a free space path with diffraction, depending if the hand is on front or behind the body, respectively, and the radiation pattern peak must be pointing away from the body. The input impedance and efficiency of the antenna will be affected by the proximity of the body, shifting, for example, the resonant frequency to values sometimes greater than the bandwidth.

In a trunk-to-trunk link surface waves are the best solution and it is necessary to have a big ground plane in order to have strong fields in it.

Only with these examples it is easy to see that the possibilities are almost infinite which make it difficult to specify ideal or general antenna characteristics.

Up to today, antenna technology has evolved very much in using textile materials as antenna substrates. The appearance of wearable antennas was required for military applications, because the soldier carrying radio would have to carry a big antenna, which could make him a priority target for enemies. Besides the issue just refereed, with the use of antennas incorporated in the uniform, many difficulties can be overcome, such as, eliminating clumsy material that can tangle in anything on the terrain. This necessity has lead to the development of an RF helmet antenna [LeTa00a] [LeTa00b] and an RF vest antenna [Abra00] [LeAd01] [Kohl04]. Both antennas are made of polyester interwoven with nickel and copper fibbers in order to make them highly conductive and dissimulated at the same time.

Wearable antennas embedded in intelligent wearable systems called “smart clothes” have potential to find a place not only in the military universe, but also in many other areas of our daily life, such as, sport outfits, medical, space applications and many others. Cloths will be able to include new features such as survival assistance in severe environment [HaHa06], as well as, new and innovative entertaining possibilities, once there will also exist wireless data communication via smart clothes.

Research on new medical imaging methods has been conducted widely because, ideally, medical screening must be non-invasive and simple to use, it must also be cheap, allow easy interpretation, minimize discomfort and provide consistent results. Future imaging methods will employ nonionizing electromagnetic waves to picture the human body, in order to detect cancer cells as early as possible [HaHa06a]. This will have appliance, for example, for detecting tumour tissues, because they have different dielectric characteristics from healthy tissues. Research is ongoing to develop better antennas for medical imaging, and textile wearable antennas that are comfortable against the skin.

When developing a wearable antenna it must be taken into account specific requirements of each application, which can be: lightweight, cheap, low-maintenance, no setup requirements and be robust. There are also important design features like selection of textile material, antenna performance that depends on material properties (e.g. wrinkle), the influence of ground plane size, effects of material conductivity, performance enhancement using electromagnetic bandgap structures, effects of the human body on the overall wearable antenna performance, including optimal positioning of the antenna on the human body and the SAR [HaHa06a].

Textile materials used as substrates can be separated in two major groups: natural and synthetic fibbers, synthetic fibbers names are usually trademarks of companies, being classified according on their typical radical, while the natural ones are those of everyday life such as cotton or wool.

Polymers are infinite molecules that repeat a certain molecular structure. According to their characteristics they can be widely used in many different applications. Some examples of synthetic fabric are fleece, upholstery fabric, vellux, synthetic felt, Cordura and Dacron.

Fleece is a synthetic woven polyester fabric, which is felted form both sides and is used to make cool-weather clothing, because it is very soft and comfortable against the skin. Polyester fibbers are hydrophobic, repelling water instead of absorbing it, drying very quickly.

Upholstery fabric is a mixture of polyester and polyacryl, woven with three fabric layers bound together. It just has 1.1 mm thickness, but its firmness makes upholstery a possible choice for antenna designs because it is harder to bend than soft fleece.

Three layers compose Vellux, the centre one is a hairy fabric that have in both sides a thin layer of foam plastic. With this the result is a soft, collapsible, flexible and insulated fabric.

Synthetic felt is similar to felt made out of wool but it is not woven or knitted and its fibbers are looser on the surface than at the centre. When deformed, which happens easily, it does not revert to its initial shape and dimensions [HaHa06a].

Delinova 200 is a fabric name, which is woven from Cordura fibbers, also known as nylon, it has very high tensile and tear strengths in the warps and wefts directions [Deli03].

Elastic properties of fabric are a very important matter, because when elastic fibbers are used as antennas substrates problems might take place. When stretched, the permittivity and thickness of the antenna alter and therefore the antenna resonant frequency changes. Stretching difficult the attachment of metallic layers on the fabric which can mean significant changes in antennas' properties dew to detached sections.

It is also important to refer that fabric antennas are used near the skin, making important the aspects of wetness of the fabric. Water can origin problems because it have much higher dielectric constant then the fabric. Moisture in an antenna makes its performance parameters to alter significantly because water will reduce the resonant frequency due to its high dielectric constant.

Chapter 3

Modelling and Simulation

This chapter provides the problem description, an overview the simulation tool used, and the chosen scenario.

3.1 Problem Description and Model

An environment near or on the body surface, is continuously changing due to movement and besides that, dielectric properties of body tissues varies from individual to individual because of many different factors such as age and anatomy. This makes it very difficult to formulate a general model for the path loss in a so adaptive environment like this one. This obligates to run simulations and tests for every different antenna because results can be unpredictable.

In this MsC Thesis, it is developed a radio channel modelling and a statistical study of the antenna characteristics. The simulation tool chosen to do these studies is *CST Studio Suite 2010*, more specifically the Microwave Studio. In Section 3.2, it is given a detailed explanation about the tool, namely the simulation method used.

Regarding the radio channel modelling, the human body model is considered to be in several body postures and for each one of those postures, two antennas are disposed in specific locations close to the body. The arrangements of the antennas were done in order to study both LOS and NLOS situations.

The statistical study, it is done by placing just one antenna in a specific body part, following a Rayleigh Distribution to vary the distances to the human body, where the most probable distance is 2 cm, as well as, a Linear Distribution in the $[0, 2\lambda]$ interval. These statistical studies provide specific information of how each part of the body influence several parameters of the antenna, such as radiation pattern and S_{11}, antenna efficiency and antenna gain.

The chosen case study for this MsC Thesis was the adult female model [ChKa09]. An adult model was chosen over the child model because a bigger model has a higher influence on the radio channel. For two antennas in the same relative position, the radio channel will have a greater length in an adult, rather than a child, and the attenuation of the signal consequently will also be higher. An adult body will also absorb more power than a child one due to its size. With all this, the adult model is certainly the best choice because in any situation, the worst case scenario must be taken into account, or at least the most probable one.

To organise the antennas around the body, it is highly recommended to divide the human body, or else, the location of the antennas may not be accurate. The division performed was made having as reference both divisions already performed by IEEE [YaSa09], [HaHa05] and the BANET Project [Bane10]. A representation of that division can be seen in Fig 3.1. The human body was divided in head, chest, waist, leg top, leg bottom, arm top and arm bottom. Besides that, when referring to the positioning of an antenna, an extra reference must be added to which one of the previous parts in order be clear where the antenna is located. That reference can be found in the left part of Fig 3.1, where is a top view of the four different possibilities. This simplifies the determination if a radio channel has LOS or does not, depending on where the antennas are located. Just by inserting all of the possibilities both in columns and rows, a connection matrix can easily be done, saying for each connection, if there is LOS or does not.

The places chosen to put the antennas were done taking into account the most suitable places to where an application, such as those referred in chapter 2, could be developed, those places are the right side of the head (HER), the chest front (CHF), on the right side of leg top (LTR) and on the left side of the arm bottom (ABL).

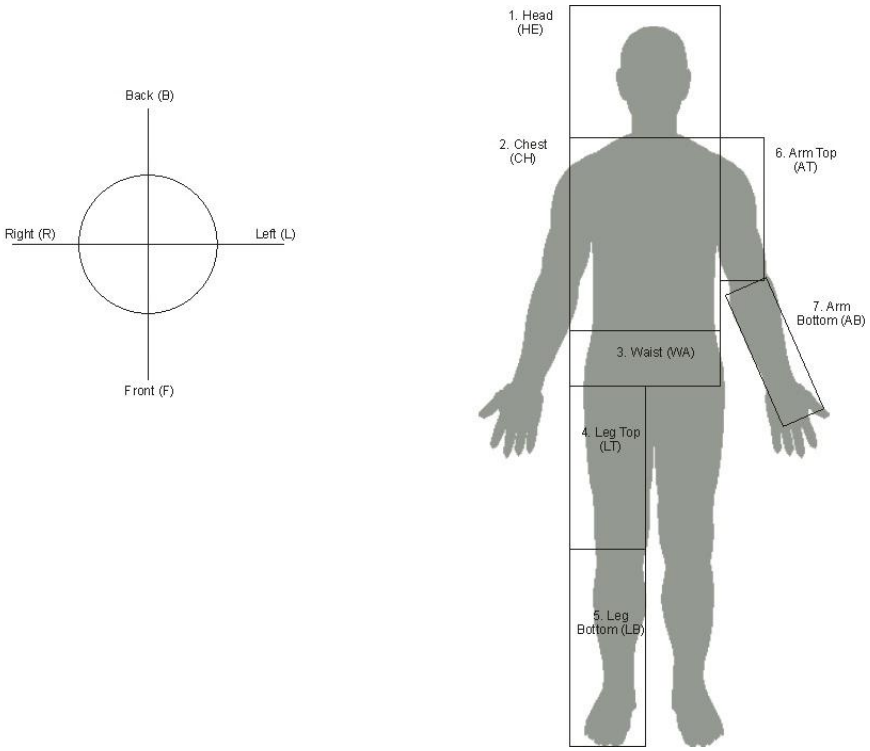

Fig 3.1. Division of the human body

3.2 CST Simulator

As any simulator, *CST Studio Suite 2010* has many features, but only some will be addressed here in order to ease the comprehension of the simulations performed.

In CST there are several Design Environments, however the only one used in this MsC Thesis is *CST Microwave Studio* once it is the more adequate one to simulate 3D electromagnetic high frequency problems. Once in *CST Microwave Studio*, it is necessary to define the units, the frequency band and the meshing. After that the antenna must be built, with proper feeding. Any desired environment, such as a body near the antennas, or a wall, can be drawn or imported.

In order to analyse the fields radiated by the antennas, field monitors are necessary. One of most important field monitors, is the *farfield monitor* because with it, it is possible to check the radiation patterns and many others antenna characteristics.

Probes might also be necessary, because they are useful to determine the value of a certain field

component in a certain position. When it is necessary to know if a certain antenna receives enough power coming from other antenna, probes are an easy way to that, however the fields components near the receiving antenna tend to change, due to the conductor materials composing it, while with a probe those changes are not taken into account.

CST uses FIT method, which consists in a universal spatial discretisation in order to solve numerically, electromagnetic field problems both in time and frequency domain. This method can be used in a wide range of frequencies.

Like FDTD, this method stands out due to high flexibility in geometric modelling and boundary handling as well as incorporation of arbitrary material distributions and material properties such as anisotropy, non-linearity and dispersion. This method uses a consistent Cartesian grid in conjunction with the leapfrog explicit time integration scheme, which was referred in Sub Section 2.3.1, leading to extremely robust algorithms with low calculation time and memory requirements that are especially adapted for transient field analysis in RF applications.

The Maxwell's integral equations that are discretised by FIT are presented here:

$$\oint_{\partial A} \mathbf{E} \cdot d\mathbf{s} = -\int_{A} \frac{\partial \mathbf{B}}{\partial t} \cdot d\mathbf{A} \tag{3.1}$$

$$\oint_{\partial \mathbf{V}} \mathbf{D} \cdot d\mathbf{A} = -\int_{V} \rho \cdot d\mathbf{V} \tag{3.2}$$

$$\oint_{\partial A} \mathbf{H} \cdot d\mathbf{s} = \int_{A} \left(\frac{\partial \mathbf{D}}{\partial t} + \mathbf{J} \right) \cdot d\mathbf{A} \tag{3.3}$$

$$\oint_{\partial \mathbf{V}} \mathbf{B} \cdot d\mathbf{A} = 0 \tag{3.4}$$

where:

- **B**: magnetic induction field
- **D**: electric displacement field
- **J**: current density
- ρ : electric charge volume density
- $d\mathbf{A}$: differential vector element of surface area A, with infinitesimal small magnitude and direction normal to surface S
- $d\mathbf{s}$: differential vector element of path length tangential to the curve
- $d\mathbf{V}$: infinitesimal differential element of volume V

To solve (3.1) to (3.4) numerically, it is necessary to define a finite calculation domain that is divided in small cell grids. Maxwell's equations are formulated for each side of the cells, as is depicted in Fig. 3.2.

Using as example (3.1), the closed integral on the equation's left side can be rewritten as the sum of all four grid components in each face of the cell. The right-hand side of the equation corresponds to the time derivative of the magnetic flux defined on the enclosed primary cell facet.

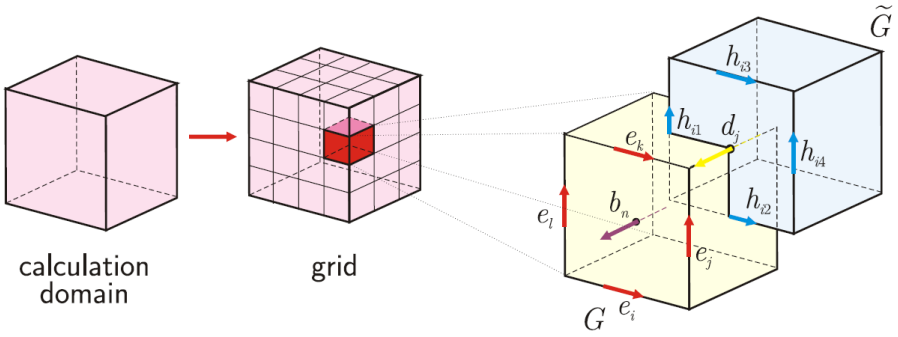

Fig 3.2. Representation the grid division and allocation of grid voltages and facet fluxes.

This course of action, for all existing cell sides, condense the calculation rule in a matrix formulation, introducing the topological matrix **C** as the discrete correspondent of the analytical curl operator as shown in Fig. 3.3.

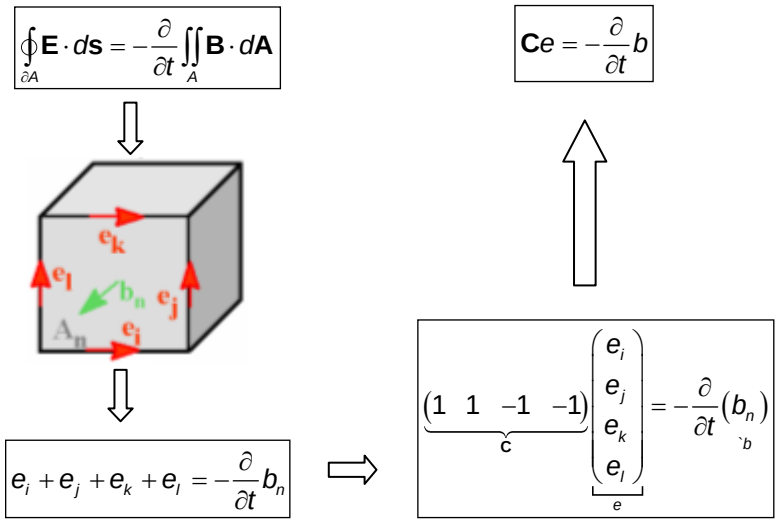

Fig 3.3. Graphic representation of the discretisation of Maxwell's integral equations (extracted from [CSTH10]).

Applying this method, from (3.1) to (3.4), it is obtained the complete discretised Maxwell's Grid Equations (MGEs):

$$\mathbf{C}e = -\frac{d}{dt}b \tag{3.5}$$

$$\tilde{\mathbf{C}}h = -\frac{d}{dt}d + j \tag{3.6}$$

$$\mathbf{S}b = 0 \tag{3.7}$$

$$\tilde{\mathbf{S}}d = q \tag{3.8}$$

where:

- **C**: discrete curl operator
- $\tilde{\mathbf{C}}$: dual discrete curl operator
- **S**: discrete divergence operator
- $\tilde{\mathbf{S}}$: dual discrete divergence operator

- b:magnetic flux
- d: electric flux
- j: electric flux density
- h: magnetic voltage
- e: electric voltage
- q: electric charge

It is important to cite that, up to this point, no errors have been introduced with the discretisation of the Maxwell's equations. One notable aspect of FIT is that important properties of the continuous gradient, curl and divergence operator are still maintained in grid space.

The spatial discretisation of a numerical algorithm can cause long-term instability. However, since the set of MGEs maintain energy and charge conservation, FIT formulation is not affected by such problems.

The missing material relations introduce numerical inaccuracy due to spatial discretisation. When defining the basic relations concerning voltages and fluxes, their integral values have to be approximated over the grid edges and cell areas, respectively. Therefore, the resultant coefficients depend on the averaged material parameters as well as on the spatial resolution of the grid and are also represented in correspondent matrices:

$$\mathbf{D} = \varepsilon \mathbf{E} \quad \Rightarrow \quad d = \mathbf{M}_{\varepsilon} e \tag{3.9}$$

$$\mathbf{B} = \mu \mathbf{H} \quad \Rightarrow \quad b = \mathbf{M}_{\mu} h \tag{3.10}$$

$$\mathbf{J} = \sigma \mathbf{E} + \mathbf{J}_{\mathbf{S}} \quad \Rightarrow \quad j = \mathbf{M}_{\sigma} e + j_s \tag{3.11}$$

where:

- $\mathbf{J}_{\mathbf{S}}$: surface current density
- j_s : surface electric flux density
- μ :magnetic permeability
- σ :conductivity
- $\mathbf{M}_{\varepsilon}$: electric permittivity coefficients matrix
- $\mathbf{M}_{\mu}$: magnetic permeability coefficients matrix
- $\mathbf{M}_{\sigma}$: conductivity coefficients matrix

The fact that the topological and metric information is divided into different equations has important theoretical, numerical and algorithmic consequences.

3.3 Resolution Assessment

3.3.1 Assessment Parameters

Given the nature of this problem, and having CST as simulator, the necessity of an optimisation assessment emerged. The two main features that must be very carefully chosen are the frequency band and the meshing.

The frequency range chosen must be as wide as possible because the solver used in the simulations is the *Transient Solver* [CSTM10]. This solver calculates fields' developments in time, so, with a wide frequency band, the excitation signal will be small in time, decreasing the time of each simulation, comparing with another simulation with a narrower band. The selection of the best meshing for the simulations is also a very important matter because, as well as the frequency band, many time and processing power may be spared.

Bandwidth and simulation time have an inverse relation but the upper frequency must not be defined randomly because the higher it is, the higher will be the number of meshcells, as it will be explained ahead. This results in a higher simulation time and more memory requirements for each simulation, meaning that a balance, between bandwidth and the maximum frequency, must be found.

In *CST Microwave Studio*, when defining the meshing, it is necessary to deal with two parameters, the Lines per Wavelength (LW) and Mesh Line Ratio Limit (RL), which can be accessed in the *Global Mesh Settings* icon. LW is a value that is associated with the wavelength of the upper frequency defined in the simulation, and is responsible for defining the minimum number of mesh cells per wavelength for all coordinate directions. RL is the maximum ratio of meshcells per wavelength that a material can have, comparing with any other, and can be defined as:

$$RL = \frac{\sqrt{\varepsilon_{rM}}}{\sqrt{\varepsilon_{rm}}} \tag{3.12}$$

where:

- $\sqrt{\varepsilon_{rM}}$: maximum refractive index
- $\sqrt{\varepsilon_{rm}}$: minimum refractive index

Materials can have different meshing because as the refractive index of a material increases, the electromagnetic waves traversing it will have a smaller velocity and consequently a smaller wavelength. This means that with a higher refractive index, a higher meshing will be obtained for that material:

$$v_{emw} = \frac{c}{\sqrt{\varepsilon_r}} \tag{3.13}$$

where:

- v_{emw} : velocity of an electromagnetic wave
- ε_r : relative electric permittivity

- c : speed of light in vacuum

Therefore, the number of meshcells, in a distance equal to the bigger wavelength, is obtained by multiplying RL by LW.

In order to select the best meshing, several parameters must be measured and compared with the reference scenario, in order to select the one that gives the best ratio between simulation time and accuracy.

To calculate radiation patterns differences, two methods were considered, an average difference and a weighted difference. The second method is important because, when comparing radiation pattern values, variations in higher power values are more important that in the lower power values once the high power direction is the angle of interest.

The values of the radiation patterns used to calculate the errors are sampled with a 5º step both for φ and θ, and ranging up to 360º and 180º respectively. The difference for a specific position was considered as:

$$\varepsilon_{pmn} = \frac{\left|G(\theta_n, \varphi_m) - G_{ref}(\theta_n, \varphi_m)\right|}{G_{ref}(\theta_n, \varphi_m)} \tag{3.14}$$

where:

- ε_{pmn} : radiation pattern relative difference in each position
- G_{ref} : reference radiation pattern value
- G : radiation pattern value
- θ_n :azimuthal angle
- φ_m : polar angle

The Pattern Average Difference (PAD) formula is as follows:

$$\delta_{AD} = \frac{\sum_{n=1}^{N}\sum_{m=1}^{M}\varepsilon_{pmn}}{N.M} \tag{3.15}$$

where:

- δ_{AD} : Pattern Average Difference
- N : total number of increments in the azimuthal angle
- M : total number of increments in the polar angle

The Pattern Weighted Difference (PWD) is:

$$\delta_{WD} = \frac{\sum_{n=1}^{N}\sum_{m=1}^{M}\varepsilon_{pmn}\cdot G_{ref}(\theta_n, \varphi_m)}{\sum_{n=1}^{N}\sum_{m=1}^{M}G_{ref}(\theta_n, \varphi_m)} \tag{3.16}$$

where:

- δ_{WD} : Pattern Weighted Difference

The other parameters that were used to select the best meshing were:

- η_{eff} : Radiation Efficiency
- G_{IEEE} :Antenna Gain
- S_{11}: Antenna Reflection Coefficient

The results for these parameters are analysed in detail in Sub Section 3.3.3.

3.3.2 Scenario

Simulations were performed in two different bands, [0.3, 2.6] GHz and [2.4, 2.6] GHz. The upper value of the bandwidth, 2.6 GHz, was chosen because it gives a reasonable margin necessary to have a resonant frequency without ambiguity. The minimum value was chosen taking into account the dielectric properties of the materials because, as can be seen in Fig. A1.1, Fig. A1.2 and Fig. A1.3, from 0.3 GHz the properties follow a trend near to linear but with small variations, except for penetration depth. Table 3.1 shows the tissues properties values for the extremes of the frequency band, being ε_r and σ the most relevant properties.

Table 3.1. Tissues properties in the boundaries of the studied frequency band.

Tissues	Frequency [GHz]	Penetration depth [cm]	ε_r	σ [$S \cdot m^{-1}$]
Muscle	0.3	5.65	58.38	0.770
	2.6	2.12	52.55	1.854
Fat	0.3	32.63	5.64	0.0396
	2.6	11.11	5.26	0.112

This is important because in CST it is very difficult, and out of context of this MsC Thesis, to insert the dependency of the dielectric properties of the materials with the frequency. With this, the dielectric properties values inserted were those for the frequency of interest, which in this case is 2.45 GHz. This simplification introduces some additional error, which was not measured.

In Fig. 3.4, it can be seen the antenna used in these simulations, which is a patch antenna with a resonant frequency in 2.45 GHz [MeCa06]. This antenna was provided by Institute of Telecommunications (IT) and was developed it a Final Report. This antenna is very adequate for this type of application because it is flat and small, which enables it to be easily integrated on clothes or equipment.

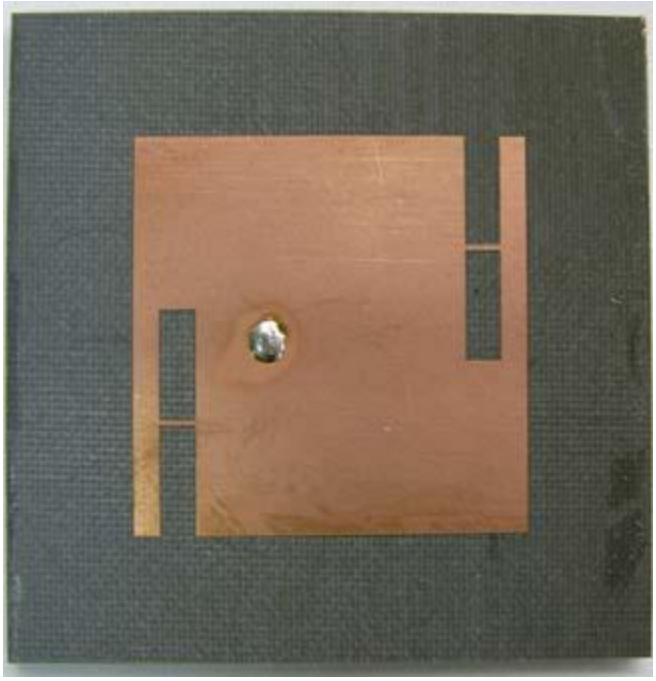

Fig 3.4. Patch antenna with switchable slots in a closed configuration (extracted from [MeCa06]).

The female adult voxel model used is from *Virtual Family* [ChKa09], but in the assessment only the head was used, in order to be possible to run the simulations in regular personal computers, due to the smaller number of meshcells. Fig A2.6 depicts how was the antenna disposed near the voxel model.

In the optimisation assessment 5 different meshing setups were compared, which are:

- LW:14 | RL:10 (14:10)
- LW:12 | RL:10 (12:10)
- LW:10 | RL:10 (12:10)
- LW:16 | RL:7 (16:7)
- LW:10 | RL:7 (10:7)

The 14:10 meshing is considered has the reference scenario, because is the one with the bigger number of meshcells and consequently more accurate values.

3.3.3 Assessment Results

In Table 3.2 it can be seen the time that each simulation took. Simulations were carried out in a regular personal computer with an Intel Core 2 Duo @ 2.40 GHz and 3 GB of RAM. During the simulations several issues were not taken into account and can introduce some minor errors in the values presented in Table 3.2, all simulations were performed with no other program running but even so the heat due to regular functioning can slow down the computer in an unpredictable way, as well as, temporary files that accumulate over time.

Table 3.2. Statistic data from the optimisation assessment

Band [GHz]	[0.3,2.6]					[2.4,2.6]				
RL	10			7		10			7	
LW	14	12	10	16	10	14	12	10	16	10
Simulation Time [s]	2033	1341	656	358	87	9870	6874	3293	1666	360
Mesh cells [10^6]	8.79	5.73	3.45	1.90	0.54	8.79	5.73	3.45	1.90	0.54
Memory [GB]	1.43	0.95	0.59	0.34	0.12	1.43	0.95	0.59	0.34	0.12

By analysing these results the chosen band to all further simulations was from [0.3, 2.6] GHz, because the simulation time was much smaller compared with the [2.4, 2.6] GHz band. The simulation time and memory required for each simulation are almost proportional to the number of meshcells, and with that, no conclusion can be made on which meshing should be selected.

Discussing antennas characteristics, first of all, it is necessary to see the influence of the human's head voxel model in the antenna characteristics. The antenna was placed right next to the left ear of the voxel model, touching it. With the introduction of the voxel model, the discrepancies obtained were:

- S_{11} increased in 2.05 dB meaning that the power reflected at the resonance frequency rose by 60.4 %.
- The gain of the antenna decreased by 1.19 dB which is -24.0 % power.
- Total efficiency of the antenna was reduced in 1 dB, meaning a loss of 20.0 %.

Radiation pattern is also affected by the presence of the head model, has can be seen in Fig. 3.5. In Fig. 3.6 can also be seen the difference in the radiation patterns for each meshing.

Radiation patterns of all simulations are presented in Fig. 3.6, showing that the major differences are in the back lobes, where the power has values between -25 dB and -12 dB, meaning that the meshing does not have a big influence in the radiation pattern. By only look to this results so far, it could seem that be best choice was 10:7 because it is the one that takes less time, but that would be a wrong choice.

Analysing Table 3.3, it can be seen that for the PAD, values are not negligible. Nevertheless by looking into Fig 3.6, it can easily be observed that the main sources of errors are the back lobes and

that the main lobes of all meshing are overlapped, showing that in the area of interest, the differences are small. With this comes the necessity of calculating a PWD.

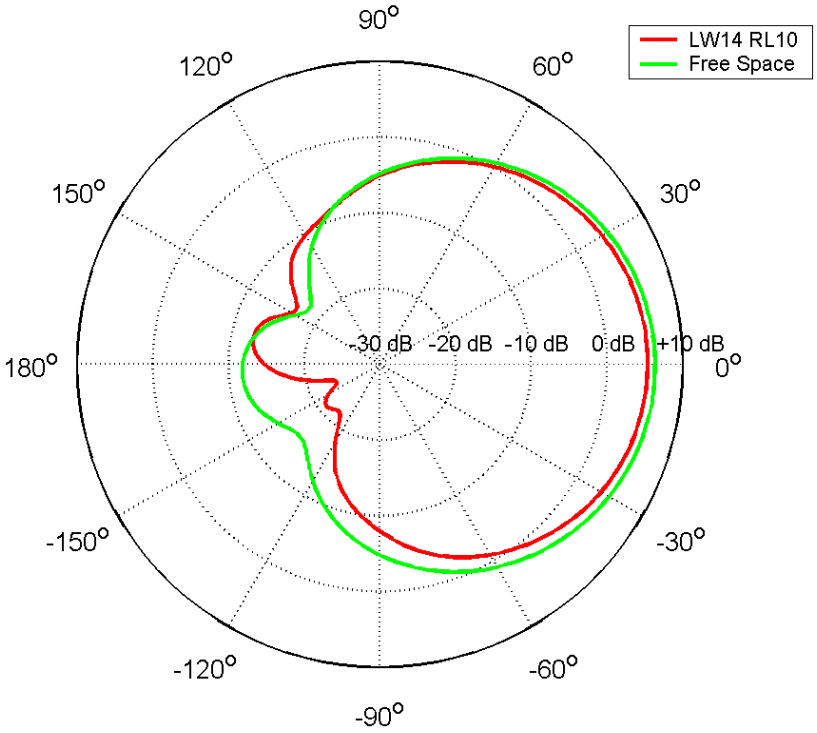

Fig 3.5. Radiation pattern of patch antenna in free space and near to the head model.

Table 3.3. Radiation Pattern Difference

LW	RL	$PAD_{[\%]}$	$PWD_{[\%]}$
14	10	0.00	0.00
12	10	2.38	0.99
10	10	5.43	1.77
16	7	3.67	1.98
10	7	12.79	10.67

In Table 3.4, are presented the values of the antenna characteristics in the presence of the body, for each meshing. As the meshing decreases, it can be seen that the differences, to the reference scenario follow a trend to increase, and for the 10:7 meshing, the results are very different from those obtained with the reference scenario. This lack of accuracy is the reason why this meshing was discarded.

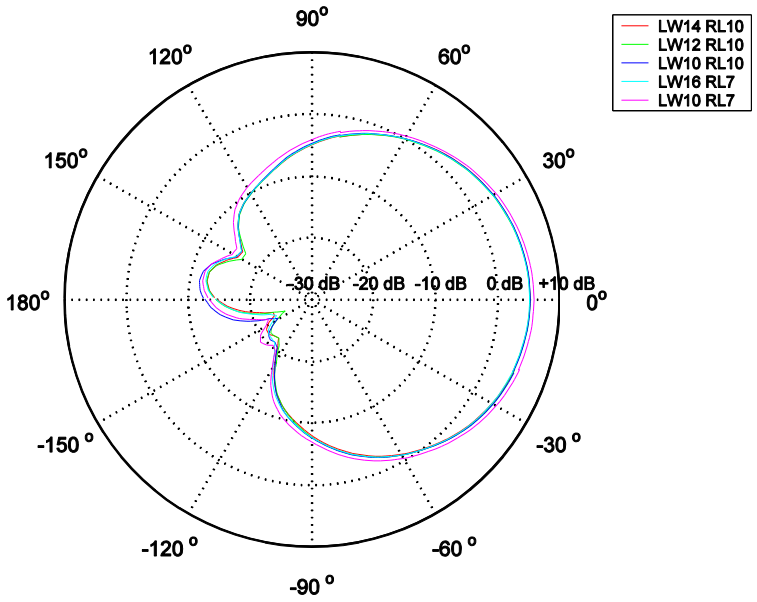

Fig 3.6. Radiation patterns of the different meshing.

In Fig. 3.7, it can be seen a chart with the relative errors, in linear values, with the information contained in Table 3.4. In linear values the differences are more obvious and easier to see, reinforcing the 16:7 selection, once the values have a difference below 5 %.

Table 3.4. Simulation results from the optimisation assessment

RL	10			7	
LW	14	12	10	16	10
S_{11} [dB]	-10.30	-10.43	-10.56	-11.49	-10.36
ΔS_{11} [dB]	—	-0.13	-0.26	-1.19	-0.06
η_{eff} [dB]	-1.93	-1.97	-1.86	-1.86	-1.85
$\Delta\eta_{eff}$ [dB]	—	-0.04	0.07	0.07	0.08
G_{IEEE} [dB]	5.39	5.37	5.47	5.34	6.00
ΔG_{IEEE} [dB]	—	-0.02	0.08	-0.05	0.61

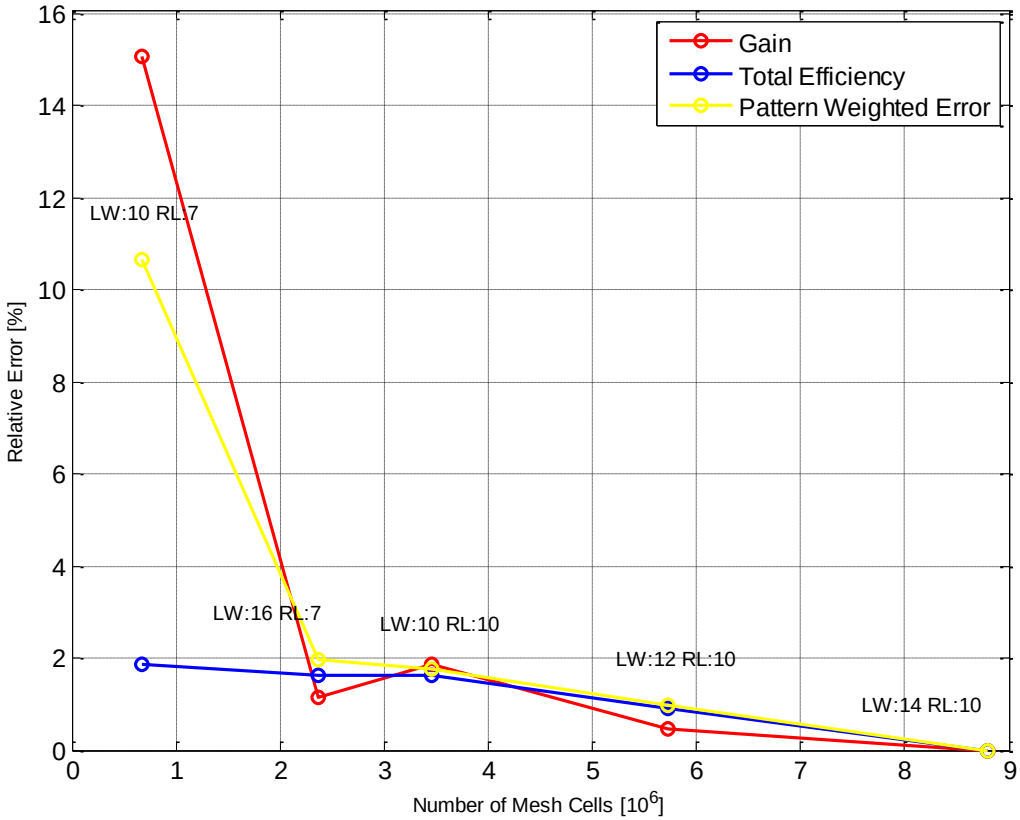

Fig 3.7. Representation of the relative errors' module for each meshing.

By comparing all four remaining meshing, because the 10:7 was already excluded, all of the parameters have small differences between them and to the reference scenario. This means that the best option to perform the simulations is the meshing that takes less time, which in this case is 16:7.

Chapter 4

Analysis of Results

This chapter provides an analysis of the data obtained from measurements, comparing them whenever possible with results from simulations.

4.1 Scenarios Definition

When performing measurements, it would be ideal to recreate the exact same conditions in a simulator, in order to compare both results. However that is impossible due to many factors, some of them associated with errors, as referred in Sub Section 2.3.2 and some others associated with available the technological resources.

Measurements were performed on three individuals, two males (CA and MM) and one female (CO). With such a small number of samples, it is not possible to do a statistical study, however it allows at least seeing how different individuals, with different anatomies, weights and heights influence the characteristics of the antenna.

In both measurements and simulations, it is used the same type of antennas depicted earlier in Sub Section 3.3.2, with a working frequency in the 2.45 GHz and antennas can be disposed on the arm, leg, chest and head.

Two sets of measurements and simulations were conducted, one with the objective of obtaining the antenna's radiation pattern in the presence of the body and the other focused on the radio channel parameters. Both of the measurements were performed in an anechoic chamber to avoid the maximum possible noise coming from the outside world and the input power of the antenna was 0 dBm, due to its proximity to the human body.

In the first set of measurements to obtain the antennas' radiation pattern affected by the presence of the human body, the antennas were positioned in the centre of the torso, as can be seen in Fig 4.1, at three different distances, 0 cm, 2 cm and 4 cm, because these range of distances are the most suitable ones for an application in this type of environment. The 0 cm distance was done by putting the antenna directly on the body, but to have it exactly at 2 cm and 4 cm it was used styrofoam with the respective thickness, taking care to make a hole in the styrofoam to pass the feeding cable. Each individual was put on top of a rotating platform and with that the full radiation pattern was obtained. To be possible to retrieve the absolute value of the field, it was necessary to perform two measurements, one to obtain the vertical component of the field and the other to obtain the horizontal component and then calculate the absolute value of the field. This was possible due to the well defined linear polarisation of the horn antenna used as probe.

Fig. 4.2 shows a sketch of the measuring setup, where can be seen that the patch and the individual rotate in the dextrosum way, from this point of view, while the horn antenna in the other side of the anechoic chamber measures the value of the field component.

The second stage of measurements had the objectives of measure the L_p of the radio channels in the vicinity of the human body, with antennas in well defined positions. The positions chosen to put the antennas in the measurements and in the simulations were the same:

- Chest Front (CHF)
- Head Right side (HER)
- Leg Bottom Right (LBR) in specific the lower right side of the right leg

- Arm Bottom Left (ABL) more accurately on the left side of the left arm in the bottom, near the wrist.

Fig 4.1. Antenna radiation pattern measurements.

Several body postures were also considered in order to see the variations in each radio channel. Figures of the body postures can be seen in Annex 3 and are the following:

- Standing up with the arm down, perpendicular to the soil (STD_ADOWN)
- Standing up with the arm parallel to the soil (STD_AFRONT)
- Standing up with the arm up, approximately 45º higher than with the arm parallel to the soil (STD_AUP)
- Standing up with the arm on the back side of the body, similar to when a person is walking and swings the arms (STD_ABACK)
- Sitting down with the arm down (SIT_ADOWN)
- Sitting down bending the elbow 90º (SIT_ABEND)
- Kneeling with just one knee on the ground and with the arms in front of the body simulating that is holding a rifle (MIL_KNEE)
- Intermediate position between standing up and knelling with just one knee on the ground as explained in the previous mark (MIL_STEP)

The calculation of L_p and the α_{pd} for all these postures were obtained, as shown:

$$L_{p[\mathrm{dB}]} = P_{e[\mathrm{dBm}]} - P_{r[\mathrm{dBm}]} + G_{e[\mathrm{dB}]} + G_{r[\mathrm{dB}]} \tag{4.1}$$

where:

- $P_{e[\mathrm{dBm}]}$: power fed to the transmitting antenna

- $P_{r[\mathrm{dBm}]}$: power available at the receiving antenna
- $G_{e[\mathrm{dB}]}$: emitting antenna gain
- $G_{r[\mathrm{dB}]}$: receiving antenna gain

and

$$L_{p[\mathrm{dB}]} = -147{,}56 + 20 \cdot \log(\mathrm{f[Hz]}) + 10 \cdot \alpha_{pd} \cdot \log(\mathrm{d[m]}) \qquad (4.2)$$

where:

- α_{pd} : average power decay

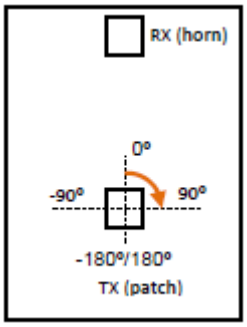

Fig 4.2. Measuring setup of the radiation patterns.

Simulations were performed using a static heterogeneous female human voxel model aged 26, with constant dielectric properties of the different tissues set up to 2.45 GHz. Figures 4.3 to 4.5 are representative of the position of the antennas in the simulations of path loss.

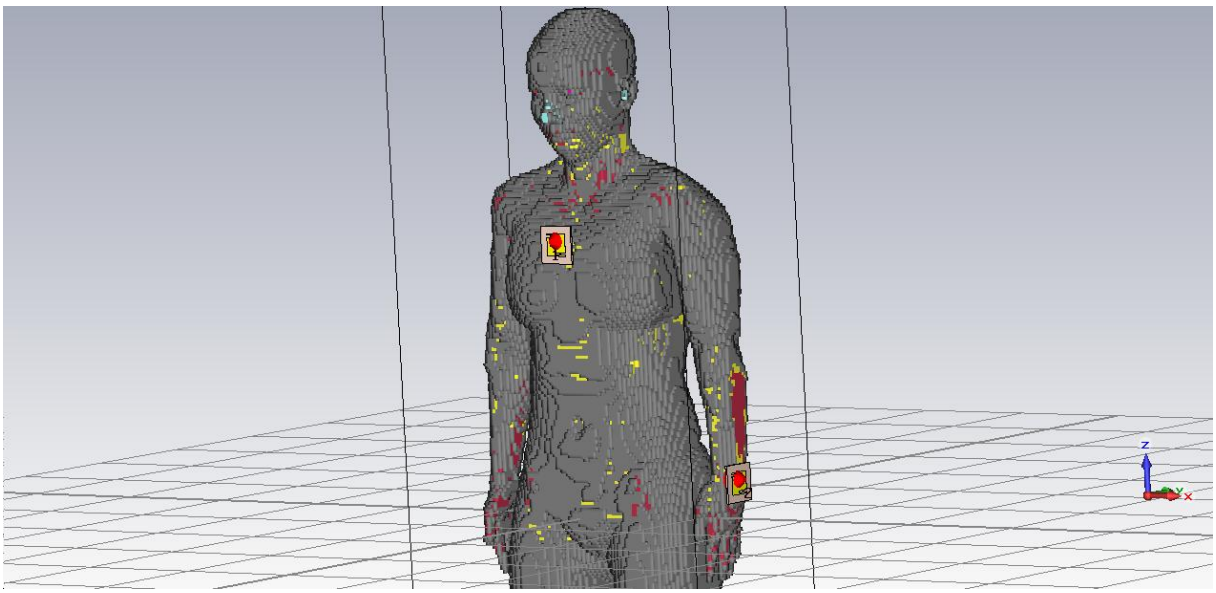

Fig 4.3. Radio link between the arm and the chest.

Due to hardware constraints, simulations were only possible to perform with parts of the human voxel model, as can be seen in Annex 2.

The antennas were placed in the same locations as in the measurements, but with the difference that it was not loaded entire voxel model, but only a portion of it, once a RAM with 3 GB is only capable of

addressing near 12 million meshcells. Radiation patterns and other antenna characteristics were simulated having just one antenna near each body part, while path loss was simulated with two antennas, also in the same setup as in the measurements.

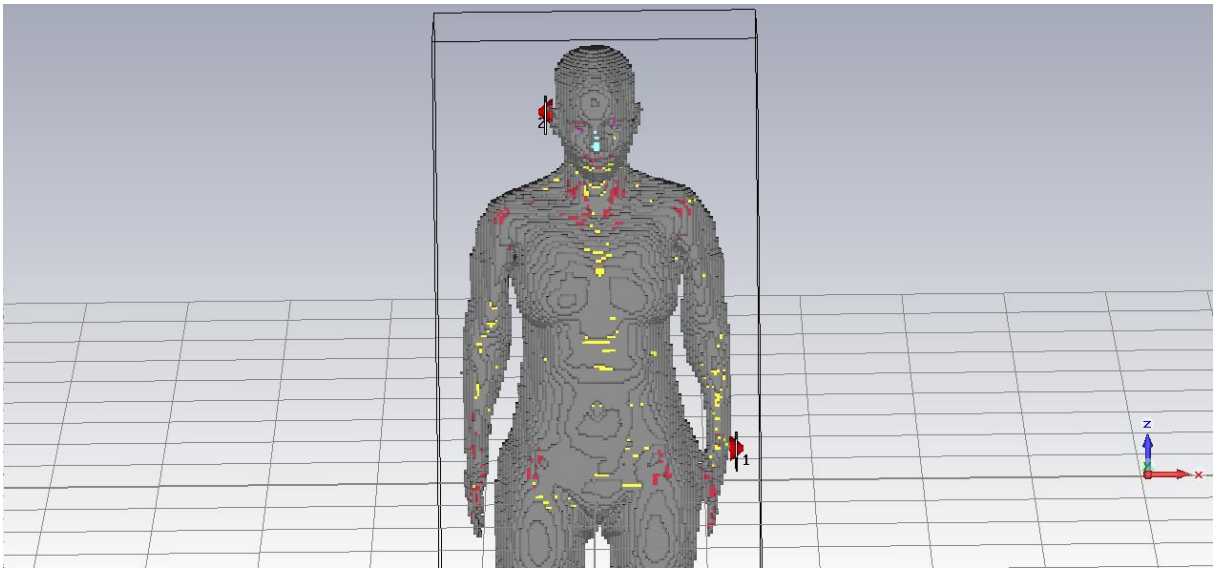

Fig 4.4. Radio link between the arm and the head.

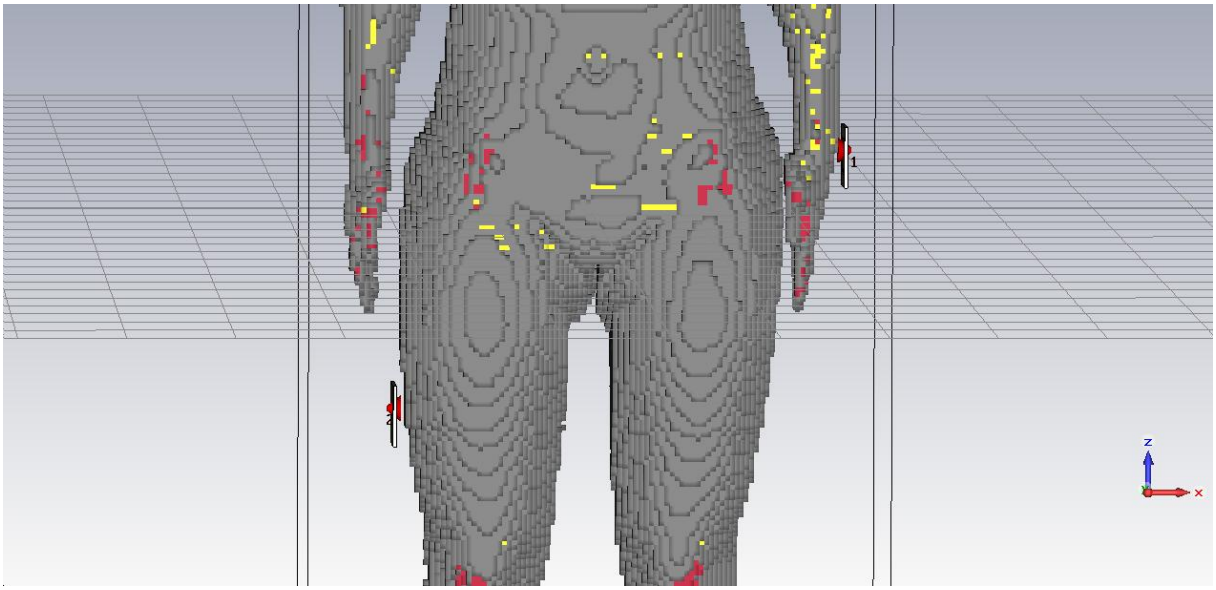

Fig 4.5. Radio link between the arm and the leg.

The figures used to present the obtained results in the Sub Chapters 4.2, 4.3 and 4.4 are bar charts, where the bars represent either the mean value obtained from 20 simulations performed for each body part, or the mean value for of all the performed measurements in a certain body posture. The line centred on each bar represents the standard deviation.

$$\bar{a} = \frac{1}{K}\sum_{i=1}^{K} a_i \tag{4.3}$$

where:

- $\bar{a}$: Mean value
- K : Number of samples
- a_i : Sample

and

$$s_K = \sqrt{\frac{1}{K}\sum_{i=1}^{K}(a_i - \bar{a})^2} \tag{4.4}$$

where:

- s_K : Standard Deviation

Table 4.1 presents the average time that all the simulations took.

Table 4.1. Time spent in simulations.

		Simulation Time [min]
Resolution Assessment [0,3; 2,6] GHz	14:10	34
	12:10	22
	10:10	11
	16:7	6
	10:7	1,5
Resolution Assessment [2,4; 2,6] GHz	14:10	164
	12:10	114
	10:10	55
	16:7	27
	10:7	6
Antenna Characterisation Rayleigh Distribution	Arm	100
	Leg	900
	Head	140
	Chest	500
Antenna Characterisation Linear Distribution	Arm	100
	Leg	900
	Head	140
	Chest	500
Radio Channel Characterisation	ABL2LBR	800
	ABL2CHF	1200
	ABL2HER	1100
Total Time		6747,5

It is important to cite that in the resolution assessment it was only performed one simulation for each meshing value, while in the antenna characterisation and the radio channel characterization twenty

simulations were performed for each. The end result is a total simulation time of more than four and a half days, being that simulations that have been redone are not taken into account, as well as the time required to design the antenna in *CST Microwave Studio 2010*.

The value of twenty simulations for each body part was selected taking into account a trade off between the time that each simulation takes and the fact that as the number so simulations increase the accuracy of the results also increases. The amount of time that each simulation took is directly proportional to number of meshcells, being obvious for example that simulations only with the arm took much less time than the simulations on the leg. Simulations were performed for resolution assessment, besides that they were also performed in all body parts with distance between body and antenna following both a linear distribution and a Rayleigh distribution and also the simulations with two antennas, which were those which took more time due to the number of meshcells.

4.2 Simulations Results

4.2.1 Radiation Patterns and Antenna Characteristics

Due to processing power limitations, the simulations were performed separately in four body parts, which were, the chest, the leg, the arm and the head. These simulations had the objective to see the influence of the body in the antenna characteristics when varying the distance between the body part and the antenna. Two sets of simulations were performed with distances following two distinct distributions with 20 samples each, a uniform distribution from 0 cm to 2λ and a Rayleigh distribution having the most probable distance of 2 cm. With a working frequency of 2.45 GHz means that 2λ represent 24,5 cm approximately.

As quoted before the positions chosen to put the antennas are as follows:

- Chest Front (CHF)
- Head Right side (HER)
- Leg Bottom Right (LBR) in specific the lower right side of the right leg
- Arm Bottom Left (ABL) more accurately on the left side of the left arm in the bottom, near the wrist.

From Fig. 4.6 to Fig. 4.9 is shown where the antennas were placed and the body parts that were used in order to be possible to perform the simulations.

In Fig. 4.10 it can be seen the antenna's S_{11} average value for each body part, as well as, in free space. When comparing with free space, the S_{11} of the antenna near all body parts tends to increase, with the exception of the chest. Besides this negative influence of the body, on average, all the values of S_{11} are smaller than the maximum acceptable value of -10 dB, meaning that even in the presence of the body, the antenna has acceptable values of reflected power, nevertheless there are results that with the variation of the distance have values above -10 dB such as the arm and the leg. In the chest,

the S_{11} value is even smaller than in free space, but that difference is certainly associated to the error contained in the models and approximations used in the simulations.

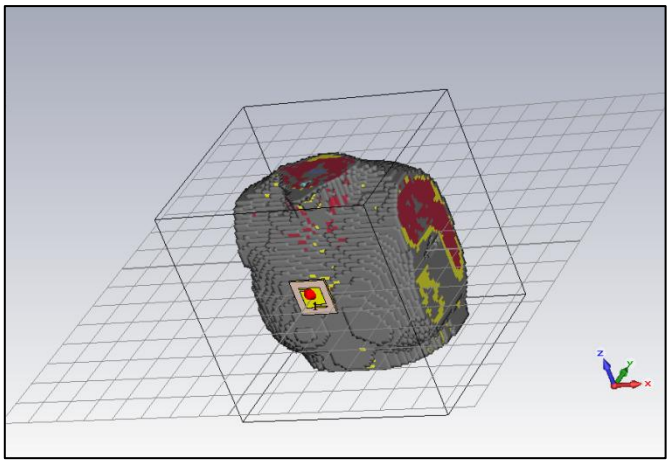

Fig 4.6. Female voxel model chest, with antenna placed in the middle of the chest.

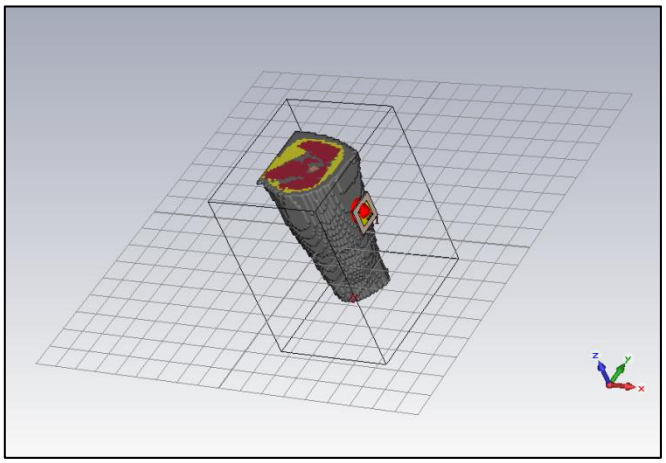

Fig 4.7. Female voxel model left leg, with the antenna placed on the left side.

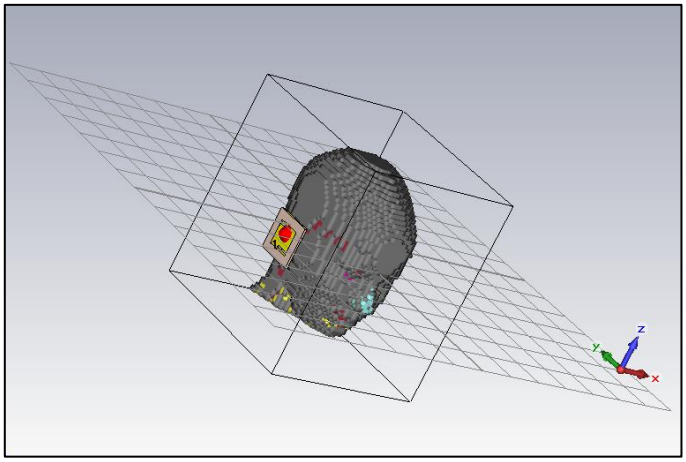

Fig 4.8. Female voxel model head, with the antenna placed on the left ear

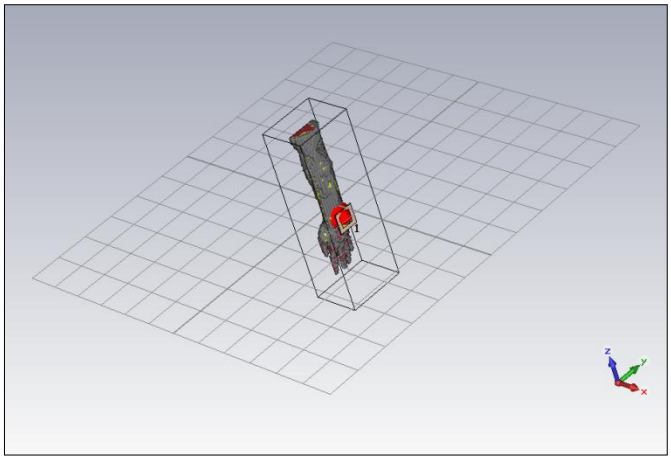

Fig 4.9. Female voxel model left arm, with the antenna placed on the wrist.

The $\eta_{eff[dB]}$ is depicted in Fig. 4.11, where it can be seen that the antenna efficiency decreases with the increase of the body part. This has to do with the size of the body part and consequently the amount of power that is absorbed by it, resulting in a smaller efficiency. The difference between the antenna efficiency in free space and the antenna near the chest is the biggest, being 0,6 dB, which represents a reduction of 10% in the antenna efficiency. Due to its central position and almost static behaviour, the chest has a very important role in BANs because many applications will have sensors on it, or at least a base station to receive the information from all sensors at send it to the backbone of the network, making it very important to take into account the effects of this body part in the antenna characteristics.

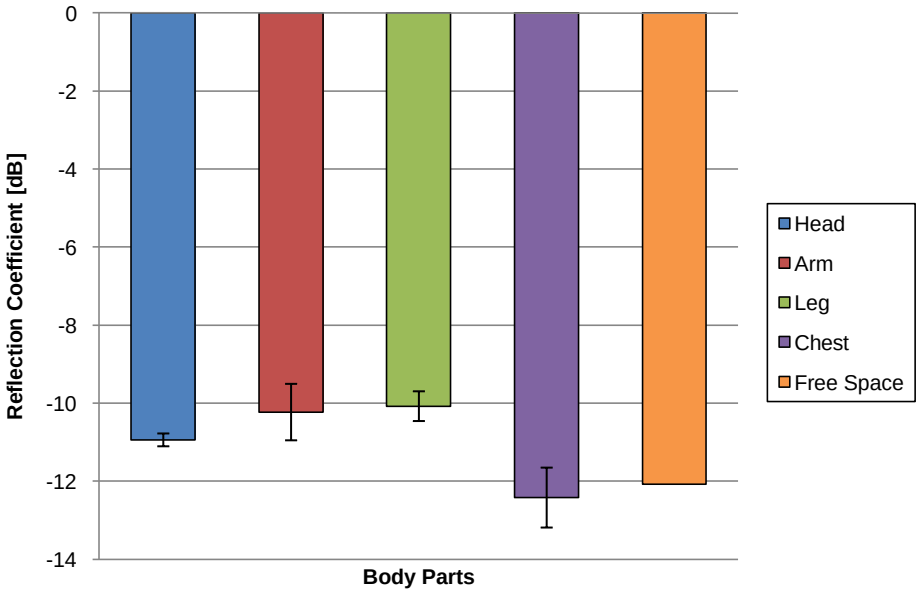

Fig 4.10. Average value of the reflection coefficient, S_{11}, for each body part, when varying the distance of the antenna from the body [0, 2λ].

As well as the $\eta_{eff[dB]}$ was obtained with a *farfield monitor*, the $G_{IEEE[dB]}$ was also obtained that way. By

observing the bar chart from Fig. 4.12, it can be seen that the antennas gain seem to decrease as the body parts get thinner, for example, the arm is the one with smaller gain and the chest is the one with bigger gain. When analysing the antenna gain it must be taken into account two factors, which are reflection and absorption of the power emitted in that direction. All of the body parts absorb power leading to a diminution of the antennas gain, however they also reflect some power, reemitting it in the opposite direction which counterbalance the effect of the absorption. In the head, the arm and the leg, the antenna gain is smaller than the one in free space, because the rays that are reflected on the body part are less than in the chest, and due to its cylindrical shape, they are not reflected in the maximum gain direction. In the chest, besides its size and consequently the amount of absorbed energy, the rays are reflected in the maximum gain direction, making it become even bigger than the gain of the antenna in free space.

In the simulations, when the antennas are touching the human voxel models (0 cm of distance), the antennas presented characteristics with uncommon values. The most likely reason is that there were materials belonging to the antenna and the voxel model that were overlapping during the simulation. The results obtained from the simulation with the arm at 0 cm were discarded due to this reason because they have no meaning and would wrongly alter the data calculated in the figures 4.10 to 4.12.

The influence of the body in the radiation pattern of the antenna, as can be seen in Annex 2, is negligible when comparing it to the radiation pattern presented of the antenna in free space. The main differences are in the back lobes, as was referred in the resolution assessment in sub chapter 3.3. The small fluctuations in the gain of the antenna, that were just referred above, and the similar shape in all the radiation patterns indicates once more that the human body does not influence greatly this antenna. Having the radiation pattern in free space as reference and comparing it with the average radiation pattern for each body part results a PWD that can be seen in Table 4.2.

The PWD in all cases is smaller than 10%, which means that the radiation patterns have small differences between them, confirming that the influence of the body parts on the antenna is negligible.

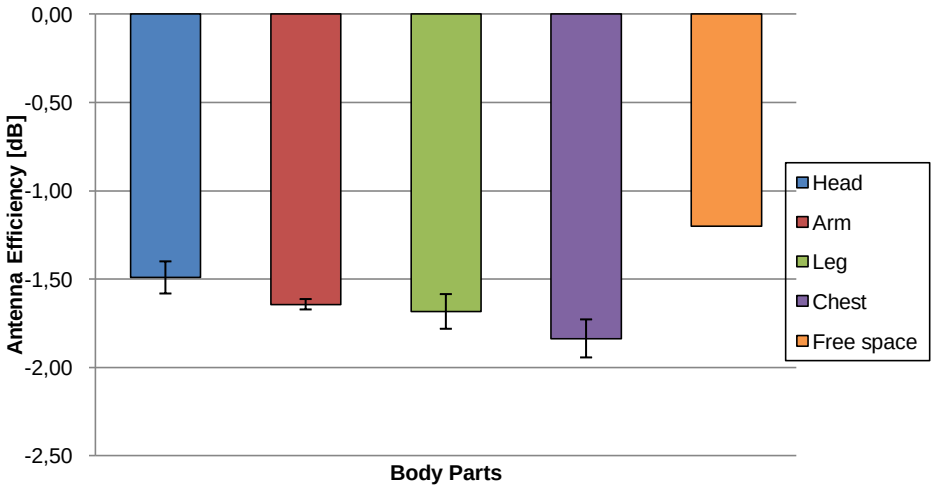

Fig 4.11. Average value of the antenna efficiency for each body part, when varying the distance of the antenna from the body [0, 2 λ].

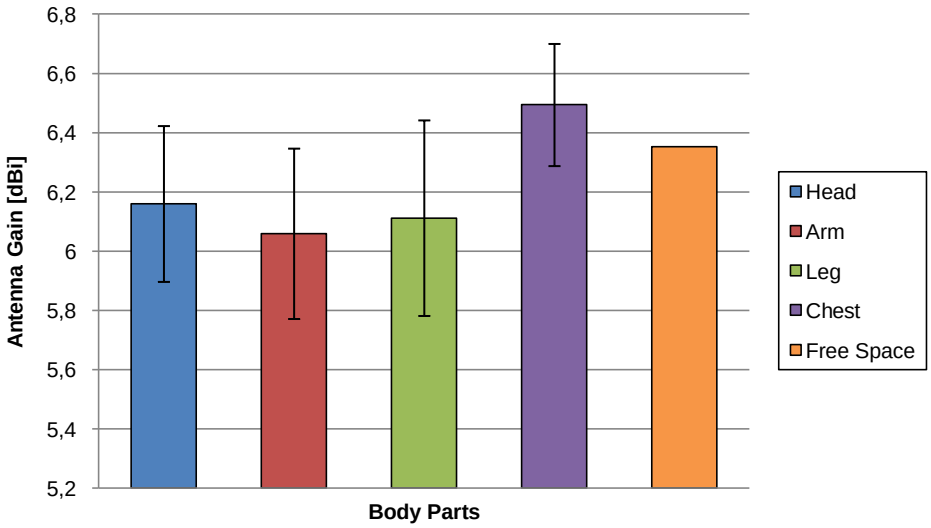

Fig 4.12. Average value of the antenna gain for each body part, when varying the distance of the antenna from the body [0, 2 λ].

Table 4.2. PWD for each body part

Body Part	$\delta_{WD[\%]}$
Arm	7,2
Chest	9,5
Head	5,2
Leg	6,7

In Fig. 4.13 are represented the radiation patterns of the simulations of each body part, depicting the one with smaller and bigger maximum direction gain from all simulated distances, the average radiation pattern radiation, as well as, with the antenna in free space. All of this enforces what has already been said, that the radiation patterns are barely affected by the presence of the body, especially in the higher gain directions, which are the most important ones

Due to the proximity between antennas and the body there is a shifting in the f_r, which can be a problem if the antennas are not working in the same frequency. However, when designing an antenna, that shifting must be taken into account and compensated, in order to the communication to become possible and to do not exist interference with other antennas or sensors that might be working in the frequency to which a certain sensor shifted to, being this reason why this antenna characteristic was not taken into account during this work.

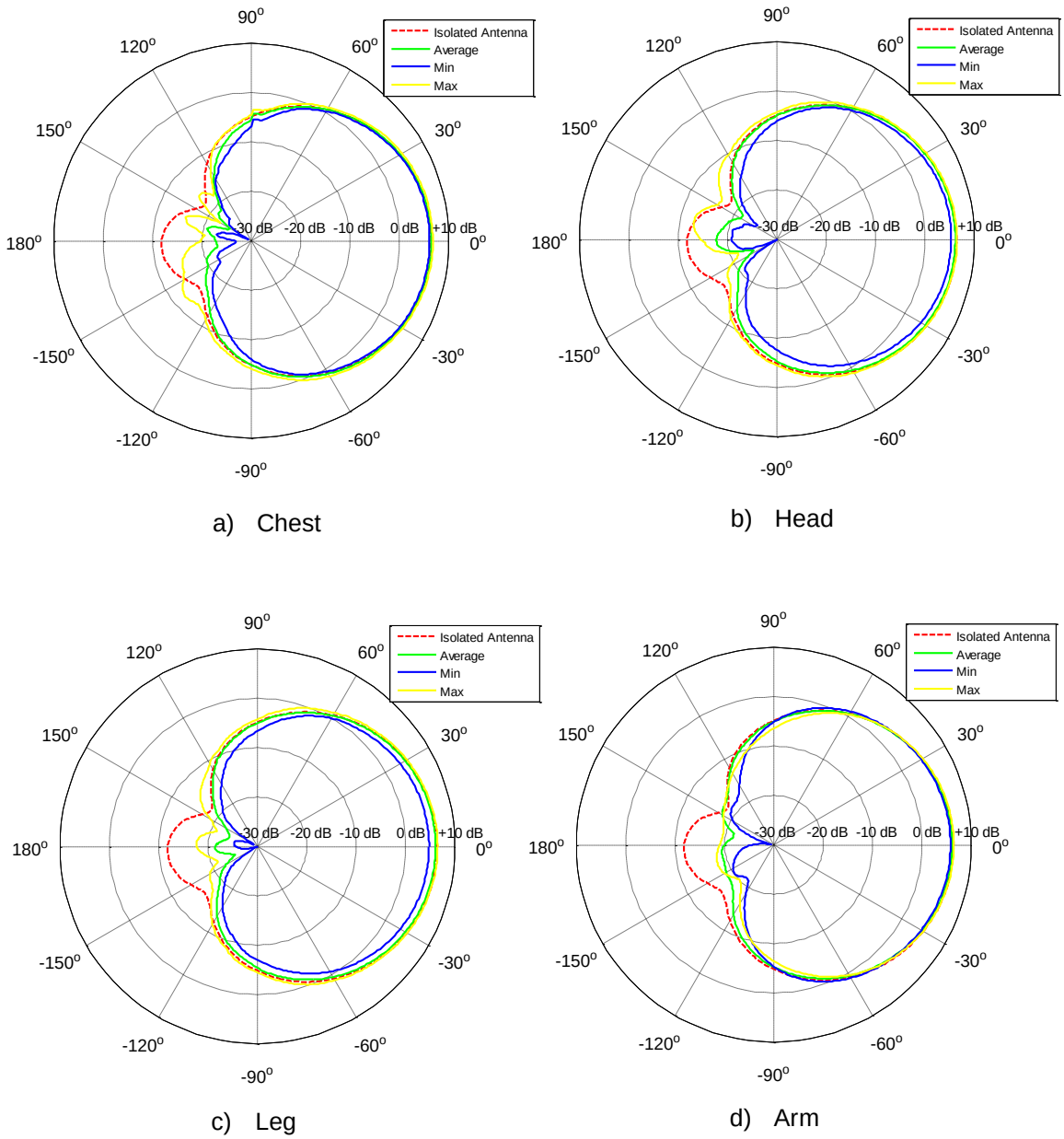

a) Chest

b) Head

c) Leg

d) Arm

Fig 4.13. Maximum, minimum, average radiation patterns near the body parts and the radiation pattern of the antenna in free space.

4.2.2 Path Loss

Simulations of the path loss were only performed with the voxel model in the STD_ADOWN position because it is not possible to grab in a voxel model and change its form, in order to simulate several positions.

The value of the G_{IEEE} used to calculate the L_p between antennas was 6,4 dB. The justification for that value is based on the information that is provided on Fig. 4.12 in Sub Section 4.2.1, which is the fact that the error associated to the simulations give no scientific meaning to values below one tenth of dB, being that this value is used in the calculations and it is considered a good approach to the real value.

Simulations were performed also only with parts of the human voxel model, but in this case had the

selection of the voxel model part had both places in where the antenna was to be placed. In the ABL2HER link, exceptionally, there was a decrease of the meshing from 16:7 to 14:7 because the distance between antennas obliges to have almost the entire voxel model. The obtained data for these simulations can only be compared with the data from measurements in the same body posture, in order to the comparison to have some meaning. Table 4.3 depicts the simulated L_p for each link, as well as, the radio channel distance.

Table 4.3. Path loss for each simulated radio link and distance between antennas.

	ABL2CHF	ABL2HER	ABL2LBR
$L_{p[dB]}$	45,61	69,07	74,84
$Distance_{[cm]}$	56,70	65,39	51,48

It can easily be seen that, for the differences in the L_p, are all dependent, both on the distance and the relative orientation between them. The ABL2LBR and ABL2HER links have approximately the same L_p, but they are the shortest and the longest radio channels respectively. The reason for this to happen has to do with the orientation of the antennas, because in the ABL2LBR link the antennas are backwards to each other, having the direction with less gain possible pointing to each other, while in ABL2HER the gain of the antenna in the direction of the other antenna is bigger than ABL2LBR. ABL2CHF has even a smaller path loss because the antenna on the chest is rotated 90º, when compared to the others, resulting in even more energy transferred through the radio link.

4.3 Measurements Results

4.3.1 Radiation Patterns

In Fig 4.14, Fig 4.15 and Fig.4.16 the radiation pattern of the antenna in free space was introduced, in order to easily observe the influence of the human body in that specific antenna characteristic, though the measurements related with this radiation pattern were performed previously, as described in [MeCa06]. In [MeCa06], there is no information about the gain of the probe antenna, or the path loss between the antennas, being the reason why it is impossible to know exactly the gain of the antenna, being that the radiation pattern is only used to make a comparison of the shape. In Fig 4.14 where is depicted the absolute value of the radiation patterns measured on CO, the female individual, and it can be seen that there are no major shape differences when comparing them with the free space radiation pattern. This happens mainly because the body is in a standing posture and the antenna has its main lobe in the direction away from the body, not affecting it, only the secondary lobes have some small differences.

A regular on-body application is very unlikely to have a distance between the body and the antenna higher than 4 cm, meaning that this antenna would be a good option, once its radiation pattern

presents no significant changes, in this range of distances.

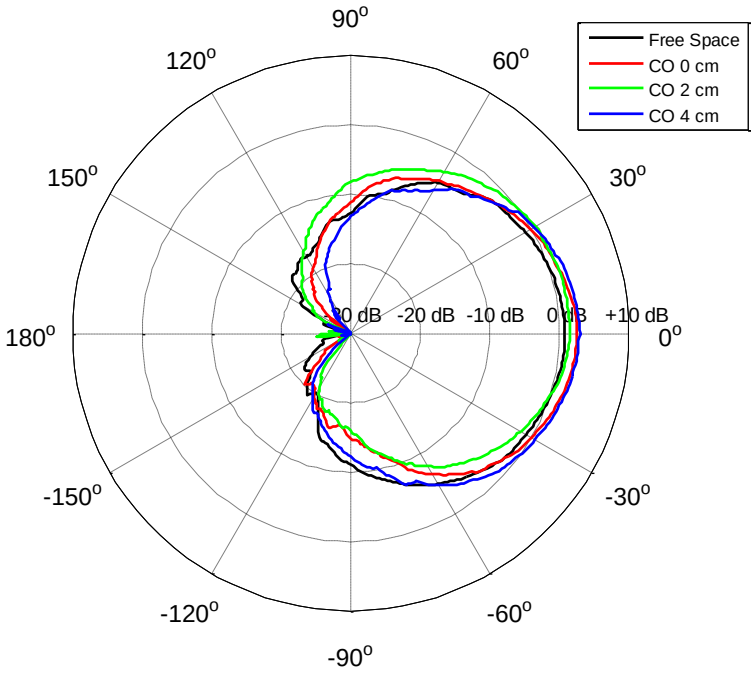

Fig 4.14. Antennas' radiation pattern on CO's body

By analysing for the other two male individuals, CA and MM, the same conclusions are obtained, as shown in Fig. 4.15.

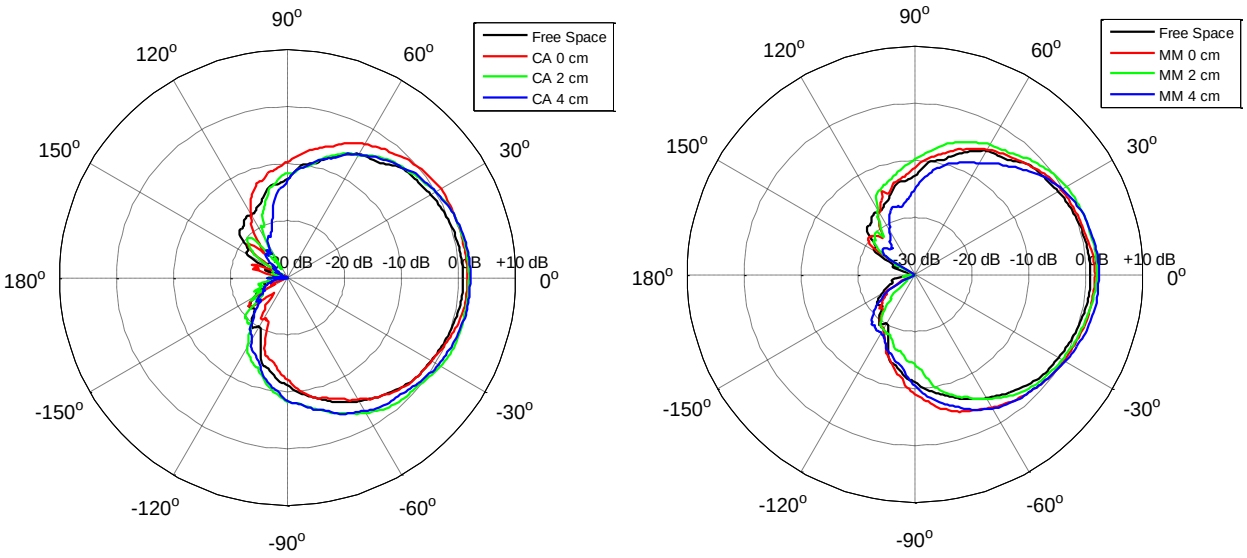

a) CA b) MM

Fig 4.15. Antennas' radiation pattern on CA's and MM' body.

Comparing the radiation patterns at the same distance for all the three individuals, it can be seen how each individual influences differently the antenna. Fig. 4.16 depicts the radiation patterns for each distance, and it can be seen that in all three distances there are also no major differences between them, because all of them have similar shapes and gains. When focusing in just on distance, all the radiation patterns seem to have one side of the lobe that irradiates more power than the other, this happens because there are no symmetrical bodies and due to the way how the antenna was placed

on the body could make it point in a direction that was not perpendicular to the body, emitting more power in that specific direction. In order to be possible to compare values, all radiation patterns were normalized and rotated to have its maximum in the 0º direction.

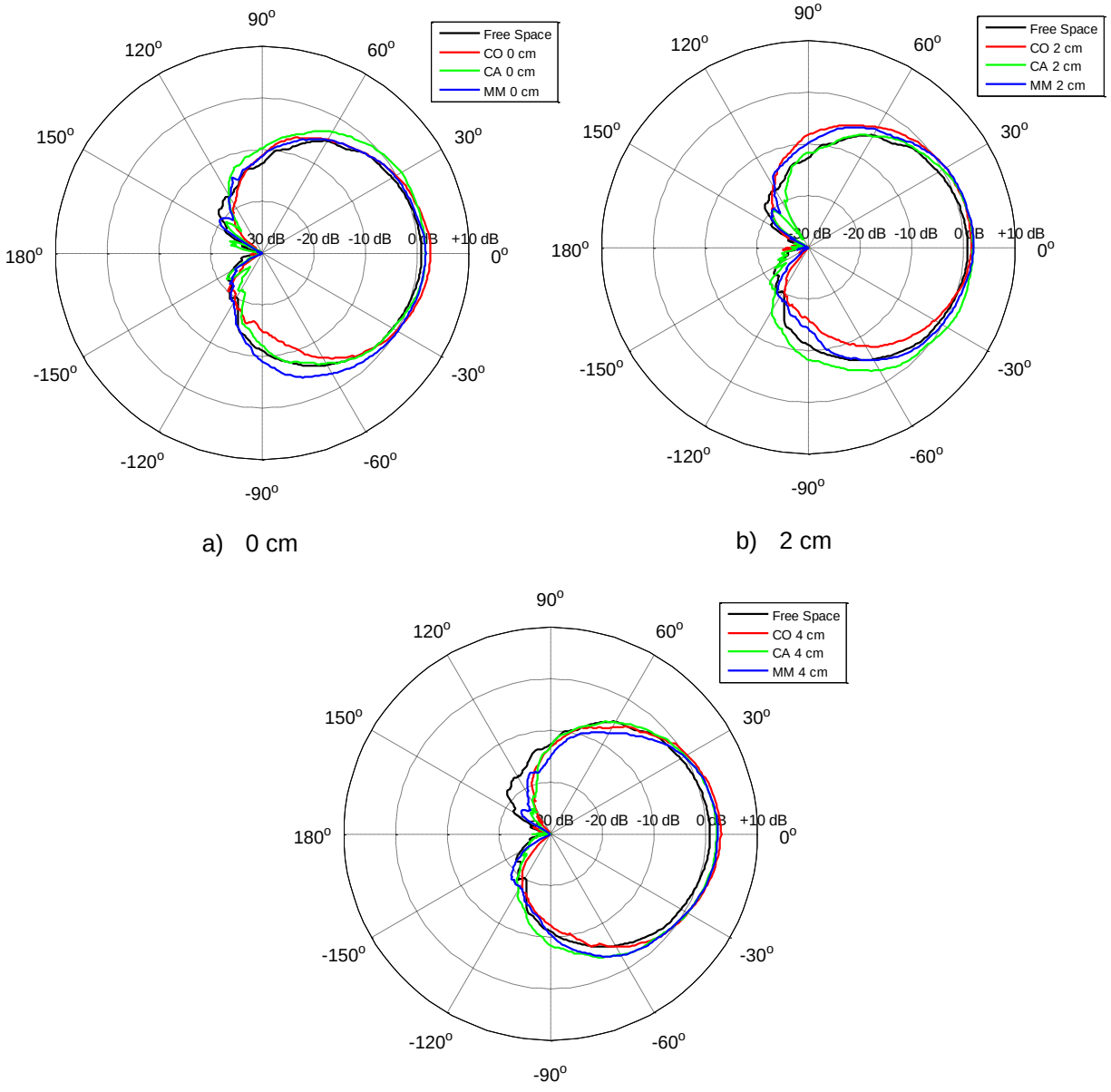

a) 0 cm

b) 2 cm

c) 4 cm

Fig 4.16. Antennas' radiation pattern at the same distance of the body.

In Table 4.4 are the PWDs for all the radiation patterns measured, taking as reference the radiation pattern measured on CO with the antenna at 0 cm. The PWDs of the measured radiation patterns are between 16% and 25%, which represents a small average difference between patterns of less than 1 dB. The PWD in the simulations was calculated taken into account the average radiation pattern for all the distances and comparing it with the antenna in free space, even so, it is possible to compare the results from the simulations of the chest.

Table 4.4. PWD of measured radiation patterns on the chest.

Individuals	Distance [cm]	$\delta_{WD[\%]}$
CO	0	0,0
	2	25,4
	4	16,1
CA	0	22,4
	2	21,5
	4	16,2
MM	0	20,7
	2	16,2
	4	17,7

4.3.2 Path Loss

Depending on the different radio channels and different individuals, the direct distance between antennas vary as shows Table 4.5. The distance was measured with a meter tape and is the smallest distance between antennas. By looking at the values it is easily seen that distances tend to be smaller with CO, however some are not, and that is due to the fact that is not possible to recreate exactly the same body posture for all three individuals, existing always differences and off course due to anatomical differences. For each body posture 3 radio channels were considered, ABL2CHF, ABL2LBR andABL2HER, which can be seen in Fig. A3.2, Fig. A3.5 and Fig. A3.6, respectively.

The S_{11} of the antenna, as can be seen from the measurements, is not greatly affected by the presence of the body because, as shown in Fig. 4.17, the differences are in the order of tenths of dBs and with small fluctuations. This means that when developing an on-body application with an antenna like the one used in this work, the S_{11} would always tend to be small and under the maximum acceptable value of -10 dB. Comparing these results with the simulations where the antennas are 2 cm away from the body, it can be seen that in the measurements the S_{11} is smaller and the values are closer to the free space one. Once more, the reason why this happens has to do with the approximations and simplifications performed in the simulations, which introduce additional errors.

As can be seen from the radiation patterns and from S_{11}, the variations of the antenna radio characteristics within different individuals are negligible, being the reason why in this Sub Section all calculations were performed using the different distances of the three different individuals, differentiating only if the radio channels have Quasi Line of Sight (QLOS) or NLOS. These measurements were also performed in the [2.4; 2.5] GHz band, with a 250 KHz step. In this work it was considered that, instead of LOS, there are QLOS once even when the antennas do not have any obstacle between them, they are not aligned with each other in the maximum power direction. In Table 4.5 is depicted the radio channel distances for each individual and body posture, while in Table 4.6 it is depicted for each radio channel if there is QLOS or NLOS. In Annex 3 there are the figures of the

body postures to help the understanding of which links have QLOS or NLOS.

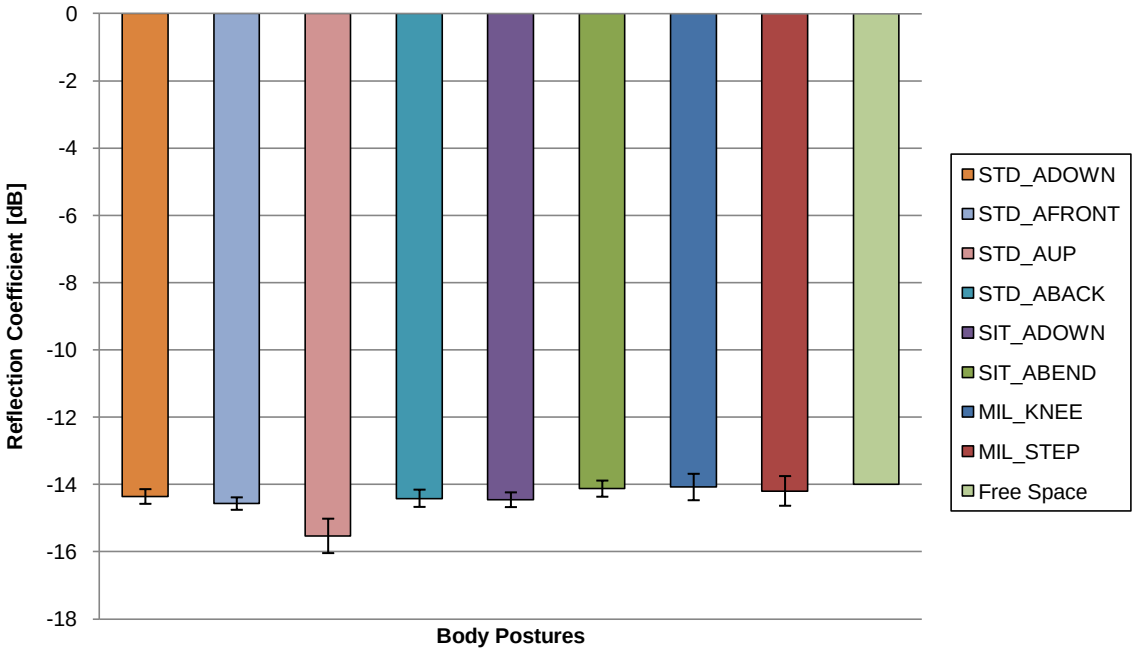

Fig 4.17. Reflection Coefficients mean values for each body posture.

In the case where the emitting antenna is in the arm and the receiving one is in the head, with the arm standing down, there is NLOS because of the shoulder.

With the arm in front there is QLOS, as well as with the arm up, but when it is standing back the entire arm and the shoulder impede to exist QLOS.

When sitting with the arm down we have the same situation as in the first one, where the individual is standing, however when the arm is bent there is QLOS.

In MIL_STEP and MIL_KNEE there is NLOS because the head is blocking the signal, once both arms are on the left side of the body, considering a right-handed individual.

When the receiving antenna is on the chest there is NLOS in the first case because of the chest itself, as well as, with the arm standing back, while with the arm in front and up there is no obstruction between the antennas.

When sitting there is NLOS with the arm down because of the body and the chair, while with the arm bent is exists QLOS.

In MIL_STEP and MIL_KNEE there is QLOS for both positions because the arm is in front of the chest making QLOS possible.

With the receiving antenna in the leg all positions have NLOS because there are always body parts obstructing the path, with exception to the one with the arm standing back.

This differentiation has the objective to develop accurate models of the path loss depending on whether it is in any one of these two situations, taking into account an associated error.

Table 4.5. Approximated radio channel distances for each individual and body posture.

		Link Distance [cm]		
		CO	CA	MM
ABL2HER	STD_ADOWN	77	90	83
	STD_AFRONT	60	68	68
	STD_AUP	50	60	62
	STD_ABACK	77	88	93
	SIT_ADOWN	70	88	81
	SIT_ABEND	58	62	62
	MIL_STEP	60	62	63
	MIL_KNEE	53	58	52
ABL2CHF	STD_ADOWN	50	46	42
	STD_AFRONT	52	50	53
	STD_AUP	56	62	64
	STD_ABACK	53	55	50
	SIT_ADOWN	37	44	44
	SIT_ABEND	33	26	30
	MIL_STEP	36	27	26
	MIL_KNEE	42	37	27
ABL2LBR	STD_ADOWN	64	73	68
	STD_AFRONT	110	130	130
	STD_AUP	142	152	148
	STD_ABACK	72	73	65
	SIT_ADOWN	76	68	79
	SIT_ABEND	67	58	65
	MIL_STEP	48	69	72
	MIL_KNEE	45	80	79

Table 4.6. QLOS and NLOS on-body paths

ABL2HER	STD_ADOWN	NLOS
	STD_AFRONT	QLOS
	STD_AUP	QLOS
	STD_ABACK	NLOS
	SIT_ADOWN	NLOS
	SIT_ABEND	QLOS
	MIL_STEP	NLOS
	MIL_KNEE	NLOS
ABL2CHF	STD_ADOWN	NLOS
	STD_AFRONT	QLOS
	STD_AUP	QLOS
	STD_ABACK	NLOS
	SIT_ADOWN	NLOS
	SIT_ABEND	QLOS
	MIL_STEP	QLOS
	MIL_KNEE	QLOS
ABL2LBR	STD_ADOWN	NLOS
	STD_AFRONT	NLOS
	STD_AUP	NLOS
	STD_ABACK	QLOS
	SIT_ADOWN	NLOS
	SIT_ABEND	NLOS
	MIL_STEP	NLOS
	MIL_KNEE	NLOS

The value of the gain of the antennas used in the calculations of the L_p is the equal to the one used in the simulations, which is 6,4 dB.

The L_p for all the radio channels can be seen in Fig 4.18, while in Fig. 4.19 the paths with QLOS and NLOS are differentiated. By analysing Fig 4.18, the human body seems to make the L_p present an α_{pd} around 4, however a more deep analysis is required, taking into account the data presented in these two figures.

When the division between QLOS and NLOS paths is taken into account as shown in Fig 4.19, it can be seen that there are different QLOS paths that have approximately the same length, but have tenths of dBs of difference, the same observation being valid to NLOS paths.

This happens due to three major reasons:

- Nearby objects, more exactly the human body
- Radiation patterns
- Body postures

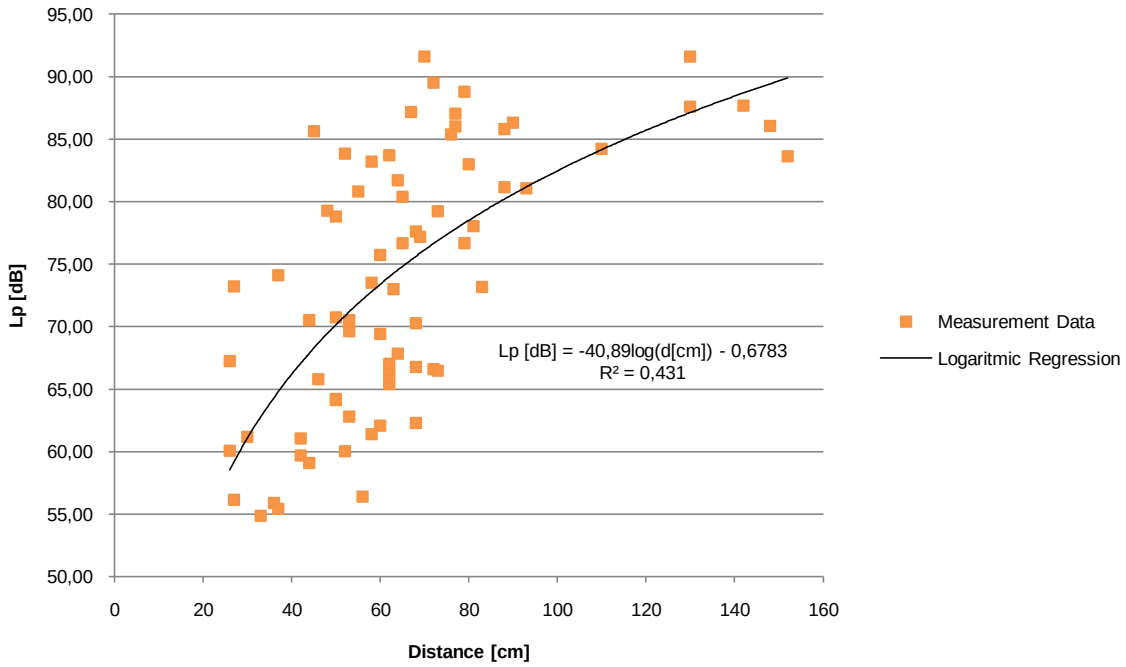

Fig 4.18. Path Loss of all the measurements performed, considering all positions and all three individuals.

The human body due to its geometry and differences from individual to individual makes it impossible to know exactly its impact on the performance of such radio channels. The signal can reach the receiver through many directions due to diffraction, with the body as an obstacle or creeping waves on the body's surface. These measurements were supposed to be performed with the individuals standing still, which is also impossible due to the necessity of breathing and any involuntary movement that is impossible to avoid.

The human body also absorbs power and the amount of energy also varies depending on the position of the antenna and on the body posture. All this factors affect the L_p in an unpredictable way as shown in Fig 4.18 and Fig 4.19.

The radiation patterns have influence on the L_p, because when calculations are made they take always into account the value of the maximum gain of the antenna. In an environment like this one, even when antennas are in QLOS, they are not pointing to each other in the maximum gain direction, which makes the gain of the antenna that is indeed applied to the radio channel to vary between smaller values than the maximum one of 6,4 dB that was considered in the calculations, resulting in more fluctuations in the L_p value.

Other aspect that is related with the radiation patterns that must be also taken into account is the body postures. For example, two individuals performing exactly the same body posture and with the antennas in the same positions, for example arm and chest, were likely to have similar L_p, ideally differing just because of the different distances. However the differences in the L_p can be substantial, just because one of the individuals put the back of the hand pointing up and the other rotate it 90º clockwise. This makes a radio channel that is considered QLOS to become NLOS increasing the L_p.

The smallest value of QLOS radio channels is 76 dBm, the individual was standing with his arm pointing back, with antennas in the arm and in the leg. Both antennas are in QLOS, but the simple rotation of the arm makes it a NLOS path, which is most suitable reason why the L_p presents this value. As well as this one, in other cases probably happened the same, such as the military position with MM, where antennas were in the arm and in the chest, that were labelled as QLOS, just have distances around 26 cm and present a L_p around 70 dBm. Other example is the standing position with the arm up with antennas in the arm and in the head, where in this case the L_p is very high both for CA and CO.

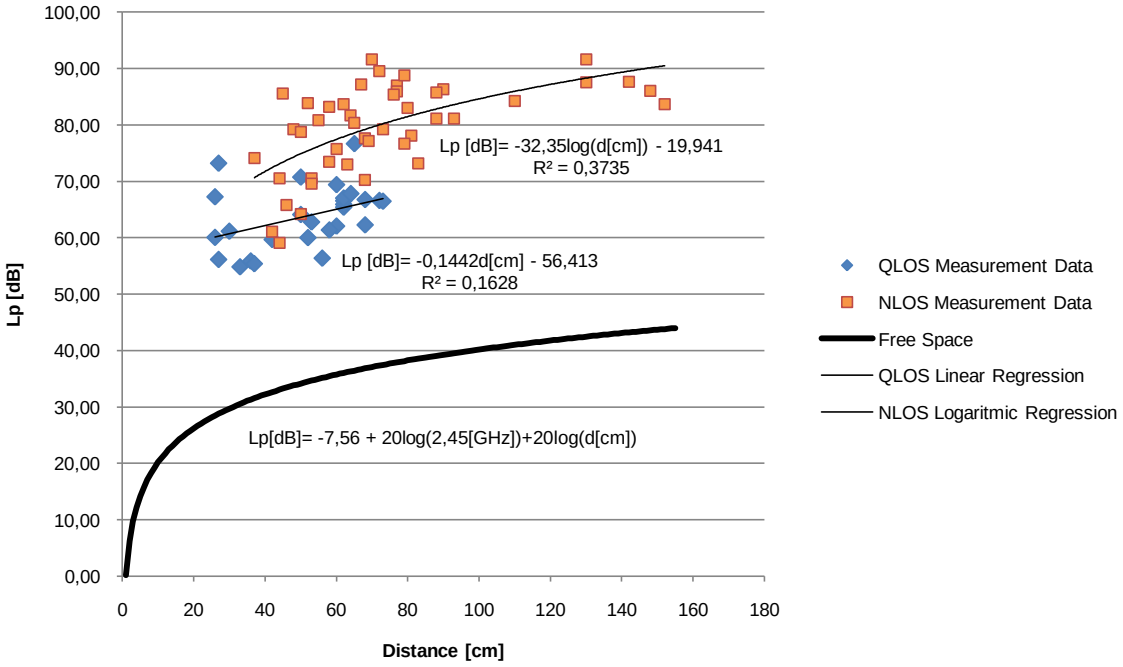

Fig 4.19. Path Loss of all the measurements performed, considering all positions and all three individuals, differentiating between QLOS and NLOS radio channels.

While there are some QLOS paths that present a high L_p, there are also NLOS paths that have a L_p smaller than expected. An example is MM with antennas in the arm and in the chest, with the arm down, both in sitting and standing up positions, in which L_p values are 10 dB above what should be expected for that distance. All these factors influence greatly and unpredictably the L_p values, being the reason why the correlation between points presents such a small value. However and besides these exceptions, in general and when considering similar distances, the values of QLOS paths present smaller values of L_p than the NLOS ones, giving nexus to the distinction that have been done.

When comparing the measured values with the theoretical L_p in free space it can easily be seen that there are a difference of approximately 30 dB to the QLOS. This difference is a result of the power that is absorbed, reflected and also due to the fact that antennas are not aligned with each other, in the maximum beam direction. To the NLOS paths, besides all the reasons referred there is also diffraction on the body surface, which increases the L_p in about 10 dB comparing with the QLOS paths.

4.4 Comparison

The radiation patterns from both the simulations and the measurements have similar shapes and values. In the measurements PWD mean value is approximately 20 %, when comparing with reference scenario, while in the simulations the mean value is close to 7 %. The PWD is bigger in the measurements than in the simulations because in the measurements it exists involuntary movement due to breathing and heart beating, all the body interacts with the antenna, while in the simulations is only a body part, there are reflections on the equipment inside the anechoic chamber and there is also noise coming from the outside of the anechoic chamber even with a good insulation.

A last comment about the radiation patterns is that with the available information, it can be seen that the antenna was not substantially affected by the presence of the body, meaning that its radio characteristics are maintained. Besides that, there is the fact that this antenna has a α_{-3dB} of more than 80º, making it a good antenna for this type of environment.

Comparing the L_p simulated with those obtained from measurements, is only possible for the data points where individuals were standing with the arm down, because of the impossibility of changing the posture of voxel models. Analysing Table 4.7, it can be seen that the path loss tends to have bigger values in the data from measurements than in the simulations, even when the distances are smaller, as can be seen for ABL2CHF. This happens because in the measurements there is a much more realistic environment, with the individuals making involuntary movements and with different body structures, with sources of noise coming from the outside world, as well as, from the measuring equipment itself. Simulations were perform in a female human voxel model, completely still and with no noise coming from anywhere, making it a much more suitable environment for a better signal reception.

Table 4.7. Simulations and measurements path loss comparison

		ABL2CHF	ABL2HER	ABL2LBR
Simulations	$L_{p[dB]}$	45,61	69,07	74,84
	Radio link distance$_{[cm]}$	56,70	65,39	51,48
Measurements	$L_{p[dB]}$	63,68	82,17	77,06
	Radio link distance$_{[cm]}$	46,00	83,33	68,33

Concerning the antenna characteristics, it is only possible to compare the S_{11}, once no other antenna characteristic was obtained from measurements. In the measurements the S_{11} has a smaller mean value of -14,5 dB and with a standard deviation of 0,5 dB for all body postures, while for the simulations, the S11 mean value is -10,9 dB and the standard deviation is 0,9 dB. This difference is justified by the simplifications made in the antenna simulations, where it is used a discrete port do feed the antenna, while in the measurements the feeding is a coaxial cable, but also due to the approximated models used in the simulations which have an associated error.

Chapter 5

Conclusions

This chapter summarises the noteworthy conclusions of the work presented. Main results are highlighted and also future work possibilities are described.

Over the past few years, telecommunications technology has evolved exponentially and since a certain level of miniaturization, it was possible the appearance of body-centric communications, which in order to be user friendly, require small wireless devices, low power consumption and considerable high data rates. This type of technology can have many strands, such as military, spatial, fitness monitoring and medical, being the reason why it typically uses the ISM band. In all of those cases the objective is the improvement of life quality of those who wear it, either because individuals have a dangerous job, such as military or police officer, by monitoring constantly their vital signs on the battlefield or on the streets, or even patient that, with these systems, do not have the necessity of be laying down in a hospital bed and can do their recover at home, or even also for the aero spatial area, to analyse how living systems respond to microgravity and spaceflight.

The emergence of BAN's and PAN's lead to the necessity of developing standards (e.g., IEEE802.15.6), being that actually there are already a large number of applications, depending on whether sensors are implanted in the body or on it, as well as many undergoing studies to know how the human body influences the radio channels between antennas and also how the power irradiated by the antennas influences the human body.

The present work has the objective to characterise the radio channel in on-body communications and can be divided in two major parts. The first one is the simulation of the antenna close to voxel models of human body parts and the second are the measurements performed in three individuals. In the first stage it was simulated the influence of each voxel models (arm, leg, chest and head) in the antenna characteristics at several distances, as well as, the radio link path loss and in the second stage it was measured the radiation pattern of the antenna in the presence of the human body, as well as, analysed the radio channel between two antennas disposed on the body, with the antennas disposed in the same places as in the simulations.

The reference scenario is a static heterogeneous female human voxel model aged 26, with a working frequency of the antennas in the 2.45 GHz and antennas can be disposed on the arm, leg, chest and head.

The simulator used in this MsC Thesis was *CST Microwave Studio* and the first step using the simulator was to decide which resolution would be the best for the data that we wanted to measure, being that this assessment was performed only with the voxel's model head and with the antenna touching the ear. Taking into account that the data required were the radiation pattern's shape and consequent antennas' gain, the S_{11}, the L_p and the f_r, there was no need for a very thin meshing because all the values obtained for all meshing, with the exception to the one with LW 10 and RL 7, were all very similar, being that the resolution chosen was LW 16 RL 7. The choice would fall into a bigger meshing if it was also necessary to measure, for example, the input impedance, due to the necessity of having a very accurate result, however with this assessment many processing time was spared and the error associated to the results obtained is still small, being below the 0,5 dB resolution of the equipment with which the measurements were performed.

Using the resolution LW 16 RL 7, all the rest of the simulations were performed for all the body parts

sampling the distances 20 times with a linear distribution from 0 cm to 2 λ (24,5 cm) and also 20 times with a Rayleigh distribution, having the most probable distance of 2 cm. With these simulations it could be concluded that the body parts do not affect considerably the characteristics of the antenna used, except for the values of S_{11} which ranges over 2 dB when comparing with the antenna in free space. In the measurements, the S_{11} have much smaller variations of 1 dB at tops, comparing in the value referred in [MeCa06]. The distance between the antenna and the human body part was sampled 20 times, because with was considered a good value, taking into account an unavoidable trade off between simulation time and accuracy of results.

The radiation patterns of the antennas, obtained in the simulations, also do not have significant variations in its shape, when varying the distance, but the maximum gain suffer small sinusoidal fluctuations due to the reflections on the body.

The proximity between antennas and the body shifts the f_r, however when designing an antenna for this type of environment, that shifting must be taken into account and compensated in order for the communication to become possible, meaning that for this work that is not an important characteristic of the antenna, being the reason why it was not taken into account during this work.

In some simulations when the distance is 0 cm, the antenna characteristics values are very different from the usual, probably because there were materials belonging to the body and the antenna, overlapping in the same space, so these values were discarded.

Comparing all body parts independently, the chest is the one that affects the most the antennas characteristics, followed by the leg, the arm and the one that affects the least is the head.

The data obtained from measurements, concerning the L_p, is widely dispersed due to many factors, such as, the fact that the distance measured for each person in each body posture, was the smallest between antennas, not meaning that that is the path through which the main part of the P_e travels. The human body itself is very irregular and heterogeneous, being very difficult to predict its influence in the antennas characteristics with an accurate equation because it would be different for each person. Movement is also an important matter because even in an individual tries to be stand still, it is impossible because there is always involuntary movement due to breathing and heart beating which also influence the results and makes the values to be more dispersed. The direction of the antennas influences greatly the results because in the calculations it was used the G_e and the G_r as being the maximum value, but that is not what happened in the measurements, once the antennas, even in LOS, were not pointing to each other in the maximum gain direction. These variations of the angles with which the antennas communicate, make the value of the antennas' gain, in that body posture, to be smaller than the maximum value and also variable.

When comparing the measured values with the theoretical L_p in free space it can easily be seen that there are a difference of approximately 30 dB to the QLOS. This difference is a result of the power that is absorbed, reflected and also due to the fact that antennas are not aligned with each other, in the maximum beam direction. To the NLOS paths, besides all the reasons referred there is also diffraction on the body, which adds an additional attenuation around 10 dB when comparing with the QLOS

paths.

The body does not affect greatly the antenna characteristics, because they only have small variations when comparing the antenna in free space and near the body is very small, however the radio channel has very big fluctuations in L_p due to the human body.

This work had some constraints to its execution, such as the limited memory of personal computers for this type of simulations, allowing only performing simulations with just a part of the body. Using the IST's workstation it would make possible the use of the entire heterogeneous voxel model and with a better meshing, in order to be possible to analyse the effect of all of the body in the antenna characteristics with more precision. It would also be a great help, software which could import a voxel model and change its posture, in order to obtain data with the voxel models for all the same positions, as in the measurements that were performed in this MsC Thesis.

As a personal opinion, I think that IST and all its students that in a near future and even further will perform any type of work related with BAN's, would have much to gain if a coordination or a partnership between IST and the two British universities existed. Both have done much more research in this area, which are the University of Birmingham and the Queen Mary, University of London. It would be good for an efficient exchange of updated information between Universities and there would not exist redundant studies to reach the same conclusions, which would result in a more efficient way to generate knowledge.

Annex 1

Dielectric Properties of Body Tissues

Dielectric properties of body tissues vary with frequency, being helpful to see its behaviour.

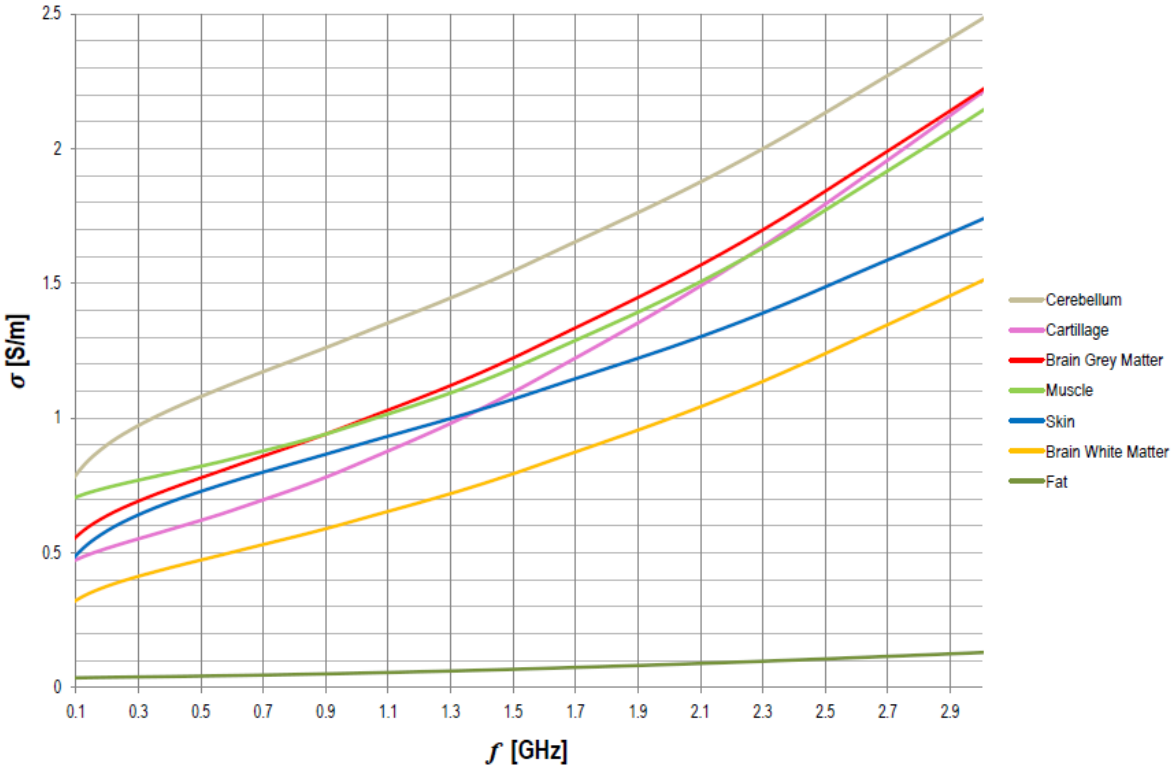

Fig A1.1. Conductivity of the most important body tissues.

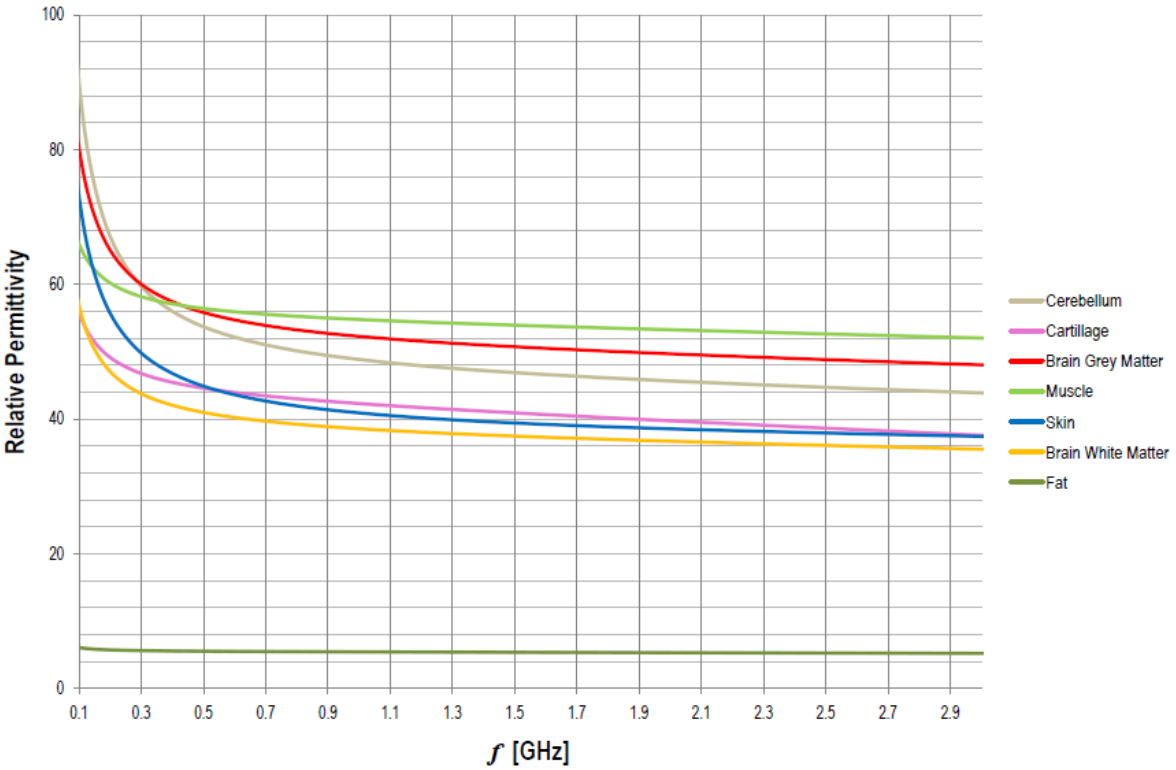

Fig A1.2. Relative permittivity of the most important body tissues.

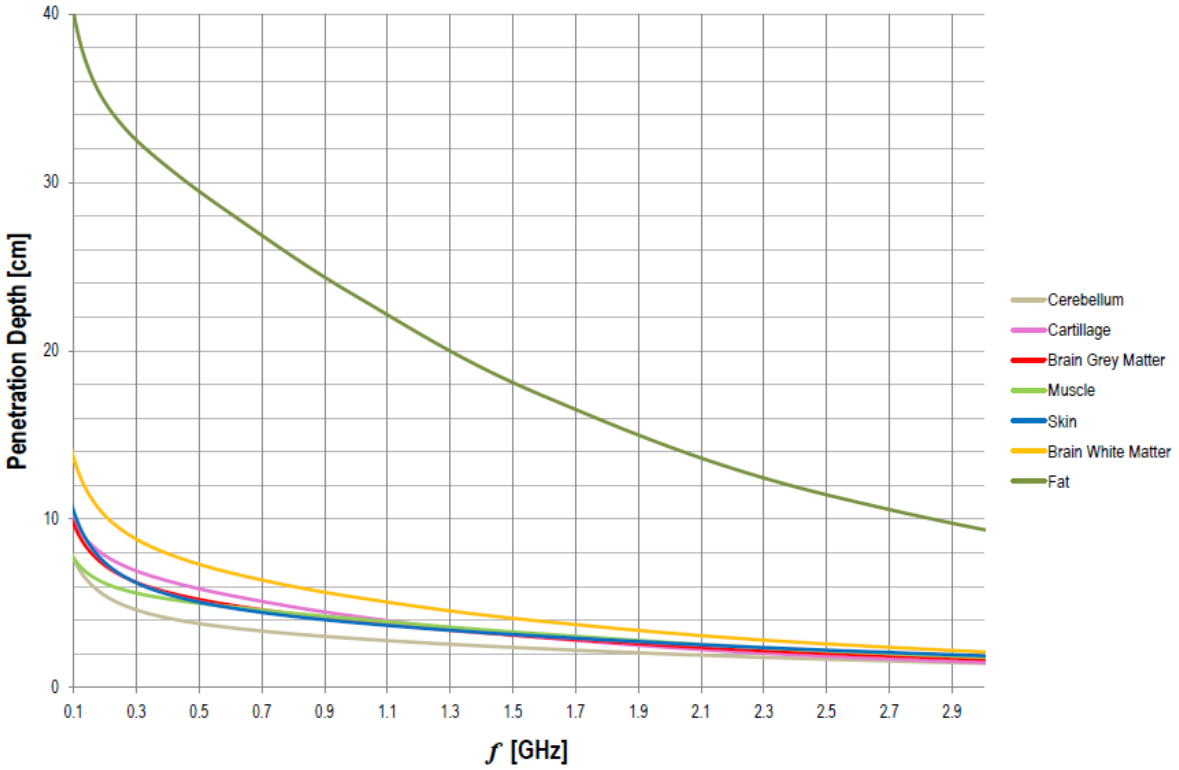

Fig A1.3. Penetration depths of the most important body tissues.

Annex 2

Voxel Models Body Parts

This annex provides the voxel models body parts considered in the simulations.

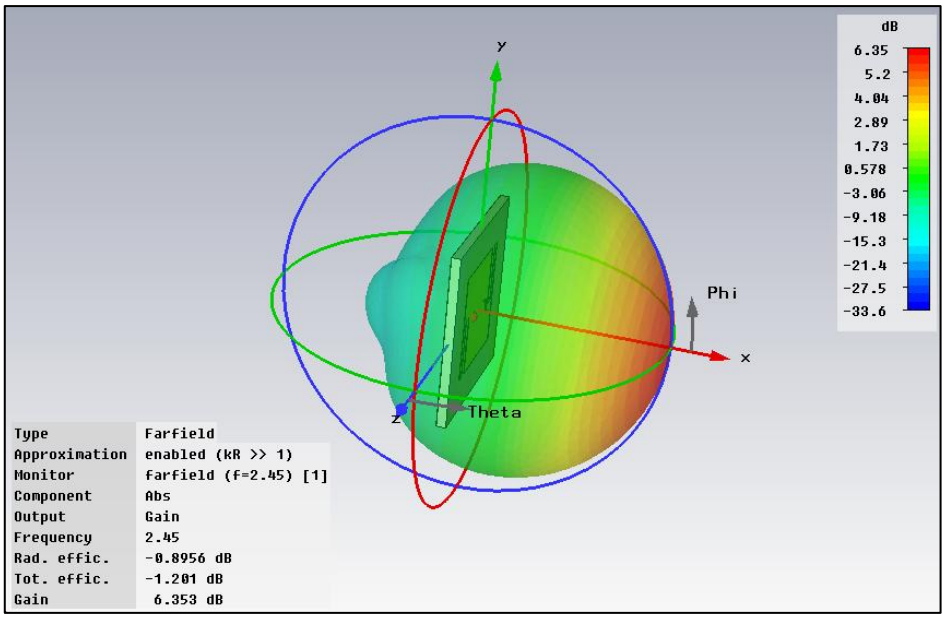

Fig. A2.1. Antennas' Radiation Pattern with antenna in free space.

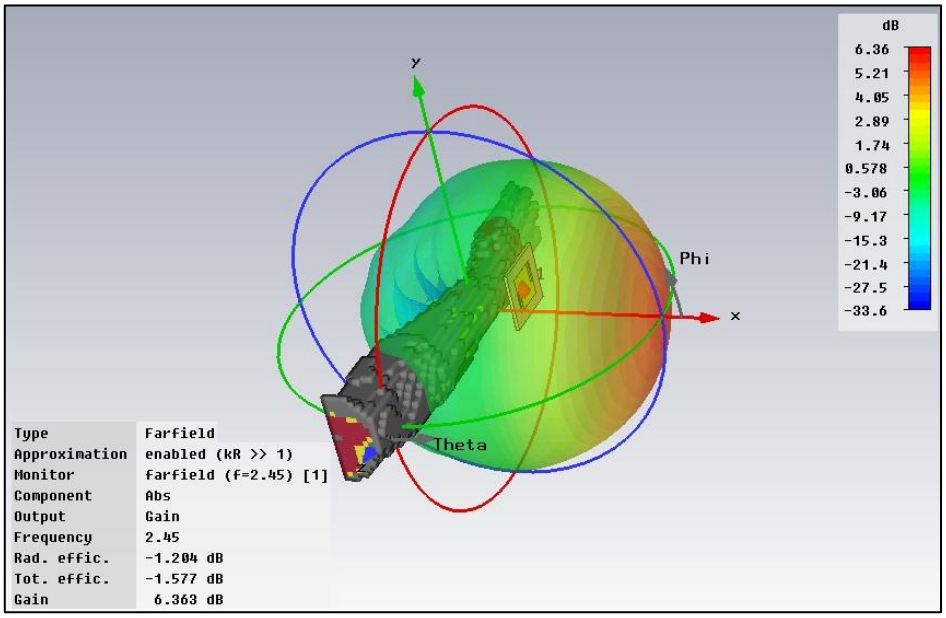

Fig. A2.2. Antennas' Radiation Pattern with antenna 12 mm away from the arm.

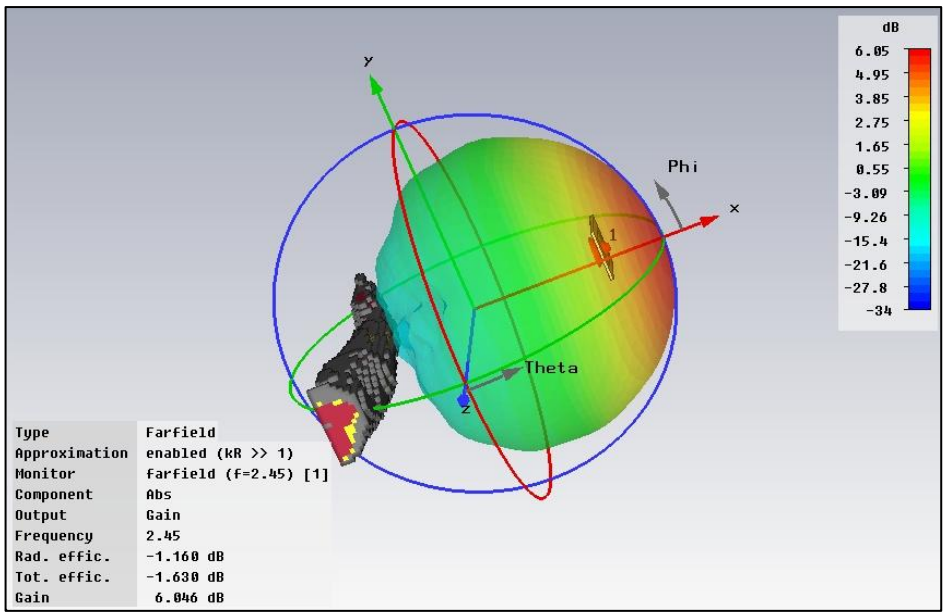

Fig. A2.3. Antennas' Radiation Pattern with antenna 2 λ (245 mm) away from the arm.

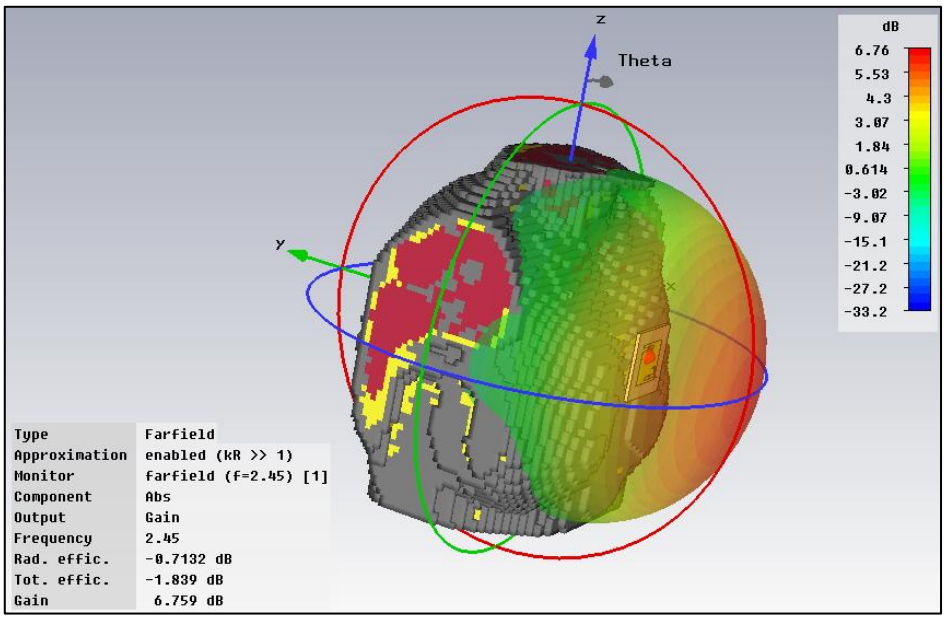

Fig. A2.4. Antennas' Radiation Pattern with antenna 12 mm away from the chest.

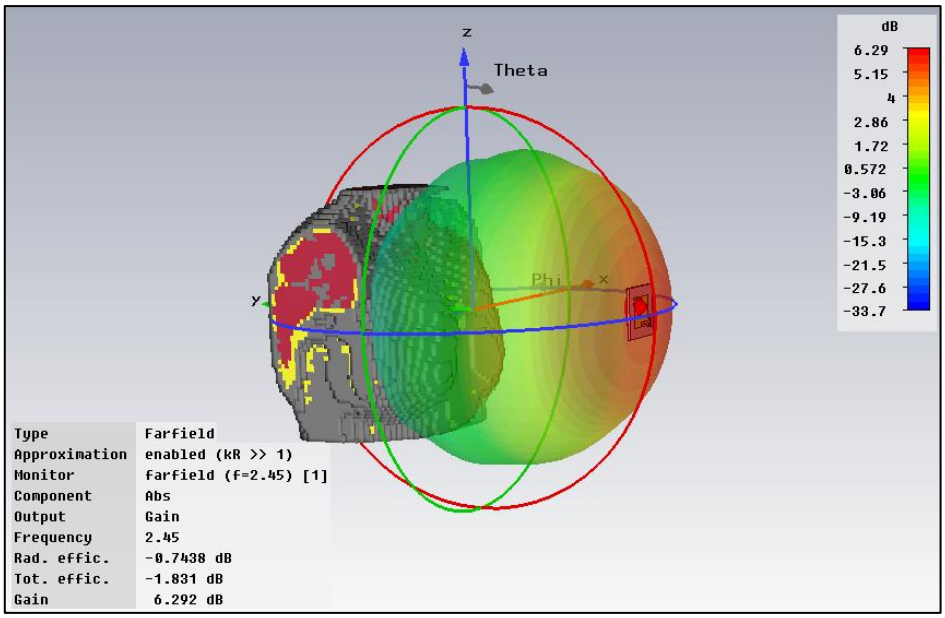

Fig. A2.5. Antennas' Radiation Pattern with antenna 2 λ (245 mm) away from the chest.

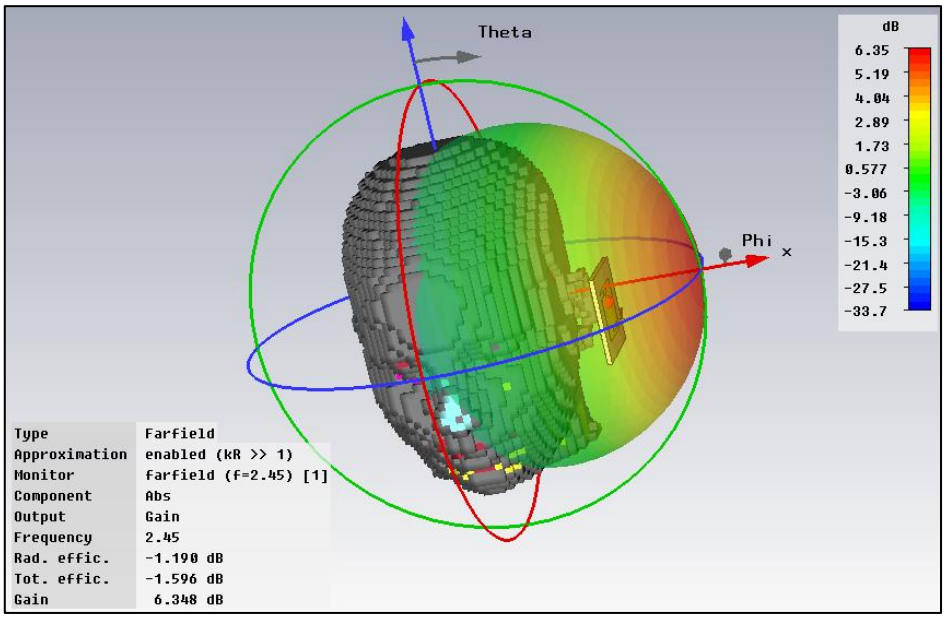

Fig. A2.6. Antennas' Radiation Pattern with antenna 12 mm away from the head.

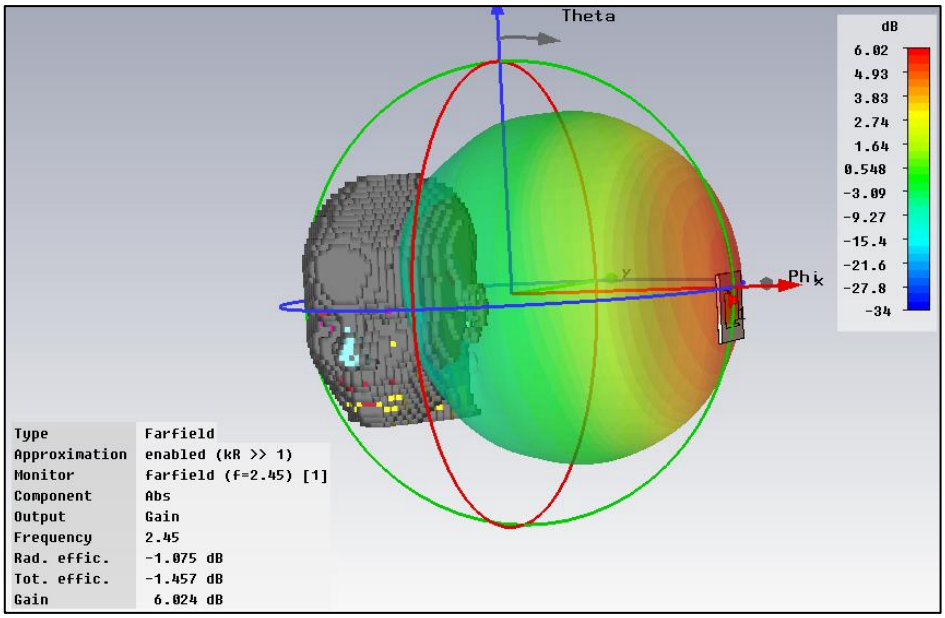

Fig. A2.7. Antennas' Radiation Pattern with antenna 2 λ (245 mm) away from the head.

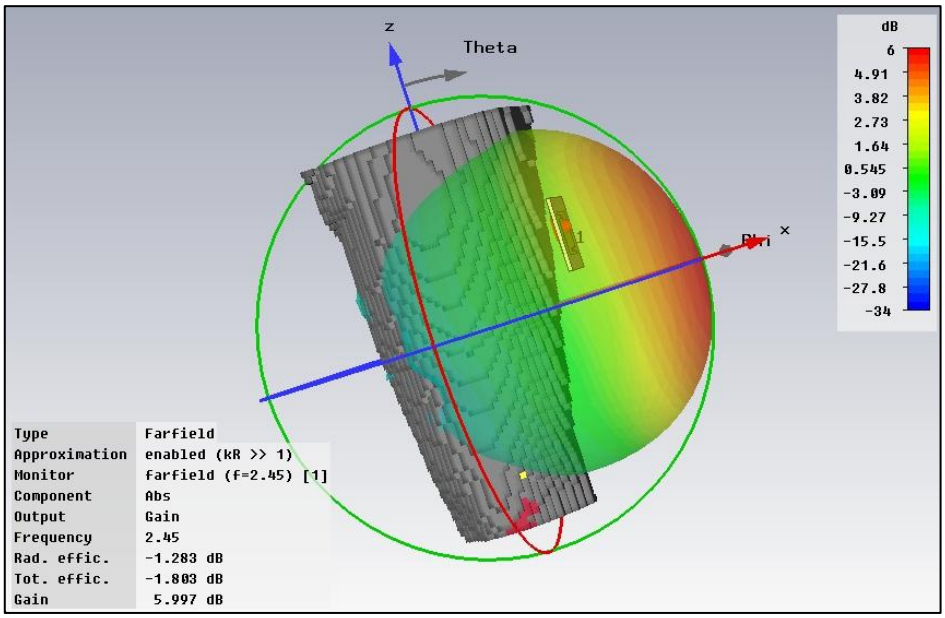

Fig. A2.8. Antennas' Radiation Pattern with antenna 12 mm away from the leg.

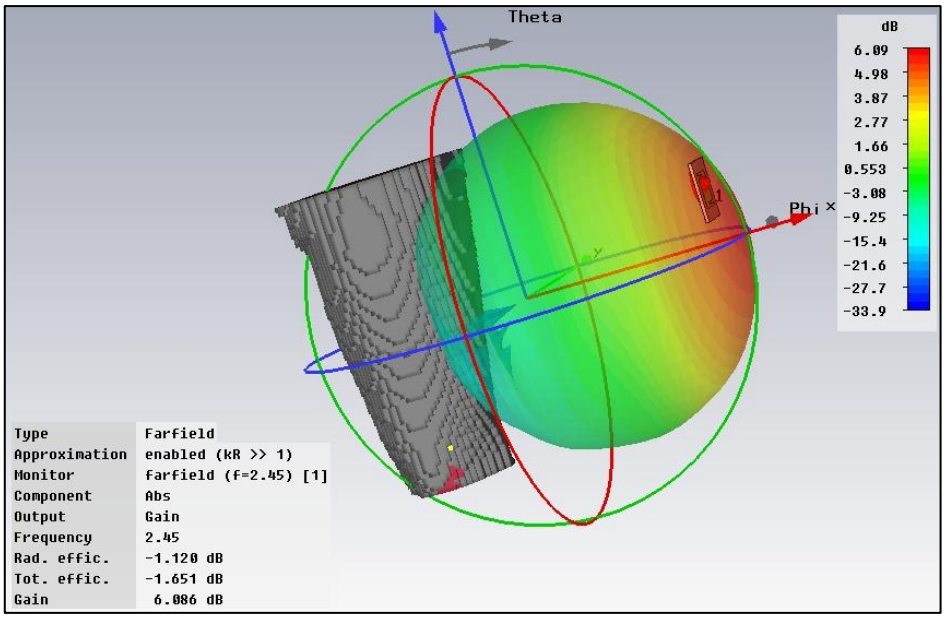

Fig. A2.9. Antennas' Radiation Pattern with antenna 2 λ (245 mm) away from the leg.

Annex 3

Different Body Postures in Path Loss Measurements

This annex provides the body postures considered in the L_p measurements.

Fig. A3.1. Standing up with the arm down, perpendicular to the soil (STD_ADOWN).

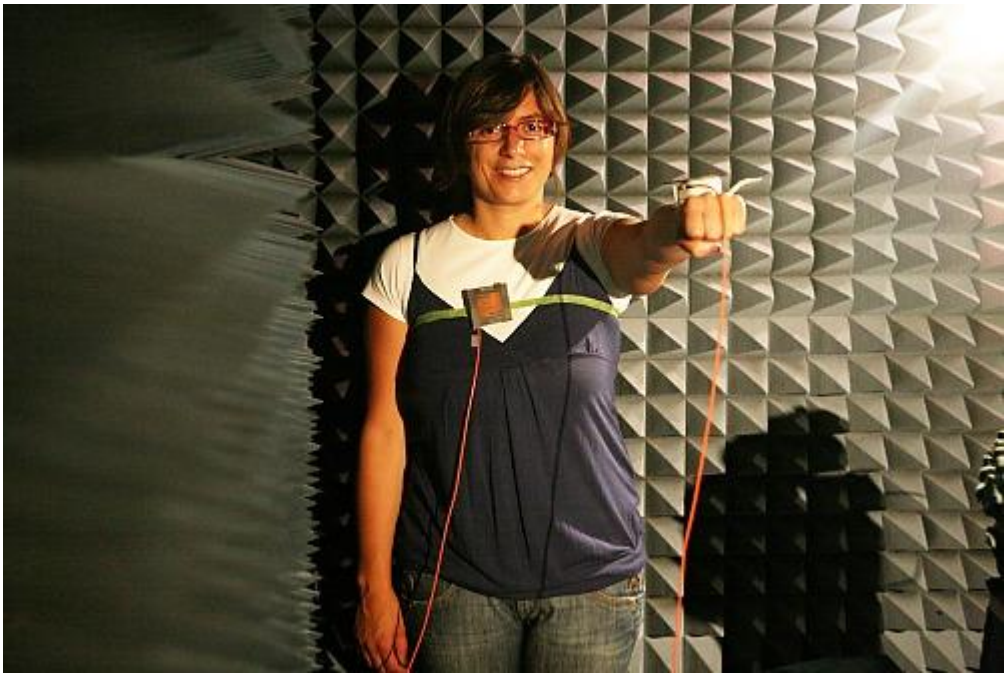

Fig. A3.2. Standing up with the arm parallel to the soil (STD_AFRONT).

Fig. A3.3. Standing up with the arm up, approximately 45º higher than with the arm parallel to the soil (STD_AUP).

Fig. A3.4. Standing up with the arm on the back side of the body, similar to when a person is walking and swings the arms (STD_ABACK).

Fig. A3.5. Sitting down with the arm down (SIT_ADOWN).

Fig. A3.6. Sitting down bending the elbow 90º (SIT_ABEND).

Fig. A3.7. Intermediate position between standing up and knelling with just one knee on the ground as explained in the previous mark (MIL_STEP).

Fig. A3.8. Kneeling with just one knee on the ground and with the arms in front of the body simulating that is holding a rifle (MIL_KNEE).

References

[Abra00] Abramo, R., et al., "*Fabrication and Testing of the COMVIN Vest Antenna*", IEEE MILCOM 2000, Vol. 2, 2000, pp. 595-598.

[Bane10] http://www.banet.fr, Mar, 2010.

[Chan00] Chang, J. T., et al., "*A Conductive Plastic for Simulating Biological Tissue at Microwave Frequencies*", IEEE Trans. on Electromagnetic Compatibility, Vol. 42, No.1, 2000, pp.76-81.

[ChKa09] Christ, A., Kainz, W., et al., "*The Virtual Family – Development of Surface-Based Anatomical Models of Two Adults and Two Children for Dosimetric Simulations*", *Physics in Medicine and Biology*, Vol. 55, No. 23, Dec 2009.

[CSTM10] CST Microwave Studio, 2010.

[Deli03] Delinova 200 of 1110 dtex DuPont's Cordura, Data sheet, Delcotex, Germany,2003.

[FaAg00] Famolari, D., and P. Agrawal, "*Architecture and Performance of an Embedded IP Bluetooth Personal Area Network*", 2000 IEEE Int. Conference on Personal Wireless Communications, December 17-20, 2000, pp. 75-79.

[Fige00] Figeys, D., "*Lab-on-a-chip: A Revolution in Bio, and Med. Sciences*", Anal. Chem., Vol. 72, No.9, May 1, 2000, pp. 330A-335A.

[HaHa05] Nechayev, Y. I. Hall, P. S. Constantinou, C. C. Hao, Y. Alomainy, A. Dubrovka, R. Parini, C. G., *IEEE Antennas And Propagation Society International Symposium*, 2005, Vol. 1B, pp. 731-734.

[HaHa06a] Hall, P. S., and Hao, Y., et al, "*Antennas and Propagation for Body Centric Wireless Communications*", Artech House, Boston/London, UK, 2006.

[HaHa06b] Hall, P. S., and Hao, Y., "*Antennas and Propagation for Body Centric Communications*", 2006)

[HaoY09] Hao,Y., "*Outlining the last developments in Body Centric Wireless Communications*", Course on Antennas and Propagation for Body-Centric Wireless Communications, London, UK, Apr. 2009.

[Harr68] Harrington, R. F., *Field Computation Moment Methods*, Macmillan, New York, USA, 1968.

[Heal10] http://www.healthyaims.org, Mar. 2010.

[ICNI98] ICNIRP, “Guidelines for Limiting Exposure to Time-Varying Electric, Magnetic, and Electromagnetic Fields (Up to 300 GHz),” *Health Physics*, Vol. 74, No. 4, 1998, pp. 494-522.

[IEEE03] IEEE, “IEEE Recommended Practice for Determining the Peak Spatial-Average Specific Absorption Rate (SAR) in the Human Head from Wireless Communications Devices: Measurement Techniques,” IEEE Std. 1528-2003, 2003.

[JimS04] Jim Stiles, *Dielectric Boundary Conditions*, University Of Kansas, University Of Kansas, USA, 2004 (http://www.ittc.ku.edu/~jstiles/220/handouts/Dielectric%20Boundary%20Conditions.pdf).

[JuTa92] Jurgens, T. G., Taflove A., Umashankar K. R., and Moore T. G., “*Finite-difference time-domain modeling of curved surfaces*”, IEEE Trans. Antennas and Propagation, vol. 40, 1992, pp. 357-366.

[Kohl04] Kohls, E. C., et al., “*A Multi-Band Body-Worn Antenna Vest*”, 2004 IEEE Antennas and Propagation Society Intl. Symp., Vol. 1, Monterey, CA, 2004, pp. 447-450.

[LeAd01] Lebaric. J. E., R. W. Adler, and M. E. Limbert, “*Ultra-Wideband, Zero Visual Signature RF Vest Antenna for Man-Portable Radios*”, IEEE MILCOM 2001, Vol. 2, 2001, pp. 1291-1294.

[LeTa00a] Lebaric, J., and A.-T. Tan, “*Ultra-Wideband RF Helmet Antenna*”, IEEE MILCOM 2000, Vol. 2, 2000, pp 591-594

[LeTa00b] Lebaric, J., and A.-T. Tan, “*Ultra-Wideband Conformal Helmet Antenna*”, IEEE Asia Pacific Microwave Conference, 2000, pp 1477-1481

[Loiz98] Loizou, P. C., “*Introduction to Cochlear Implants*”, IEEE Signal Processing Magazine, September 1998, pp. 101-130.

[MeCa06] Medeiros, C., Castela, A. M., *Reconfigurable Antennas for Multi-Services* (in Portuguese), Final Report, Instituto Superior Técnico, Lisboa, Portugal, 2006.

[Ming03] Mingui, S., et al., “*Data Communication Between Brain Implants and Computer*”, IEEE Trans. On Neural Systems and Rehabilitation Eng., Vol. 11, No. 2, June 2003.

[NiKi96] Nikawa, Y., M. Chino, and K. Kikuchi, “*Soft and Dry Phantom Modeling Material Using Silicone Rubber with Carbon Fiber*”, IEEE Trans. on Microwave Theory and techniques Vol. 44, No. 10, Part 2, 1996, pp. 1949-1952.

[Perr93] Perrins, J., “*Types of Sensor for Rate Responsive Pacemakers*”, IEEE Colloq. On Int. Cardiac Implants, January 29, 1993.

[Rant00] Ratanen, J., et al., “*Smart Clothing for the Arctic Environment*” IEEE 4th Int. Symp. Wearable Computers, 2000, pp. 15-23.

[Reic09] Reichman, A., “*Body Area Networks: Applications and Challenges*”, COST 2100 TD(09)717, Braunschweig, Germany, 2009.

[Schw02] Schwendener, R., "*Indoor Radio Channel Model for Protocol Evaluation of Wireless Personal Area Networks*", 13th IEEE Int. Symp. Personal, Indoor and Mobile Radio Communications, Vol.2, September 15-18, 2002, pp. 891-895

[SmSi93] Smailagic, A., and Siewiorek D. P., "*A Case Study in Embedded-System Design: The VuMan 2 Wearable Computer*", IEEE Design Test Computers, Vol. 10, No.3, September 1993, pp. 56-67.

[Stra03] Stratis, G,. et al., "*Composite Antenna Pattern for realistic Ray Tracing Simulations*", IEEE Antennas and Propagation Society Int. Symp., 2003.

[Stuc80] Stuchly, M. A., and S. S. Stuchly, "*Dieletric Properties of Biological Substances-Tabulated*", J. of Microwave Power, Vol. 15, No. 1, 1980, pp. 19-26.

[Tafl95] Taflove, A., "Compu*tational Electrodynamics The Finite-Difference Time-Domain Method*", Artech House, Boston/London, UK, 1995.

[Tamu97] Tamura, H., et al., "*Dry Phantom Composed of Ceramics and Graphite Powder*", IEEE Trans. on Electromagnetic Compatibility, Vol. 39, No. 2, May 1997, pp.132-137

[Weil77] Weiland, T., A Discretization Method for the Solution of Maxwell's Equations for Six-Component Fields, Electronics and Communications AEUE, vol. 31, no. 3, pp. 116–120, 1977.

[Wica10] http://www.wica.intec.ugent.be/research/wireless/body-area-networks, Sep. 2010.

[YaSa09] Yazdandoost, K. Y. and Sayrafian-Pour, K., Channel Model for Body Area Networks, IEEE P802.15 Working Group for Wireless Personal Area Networks (WPANs), 2009.

[YeeK96] Yee, K. S., "*Numerical Solution of Initial Boundary Value Problems Involving Maxwell's Equation in Isotropic Media*", IEEE Trans. On Antennas and Propagation, Vol. 14, No.3 pp. 1996, 302-307.